Final Technical Report to the National Aeronautics and Space Administration for the

DART

Double Asteroid Redirection Test (DART) Mission

October 2023

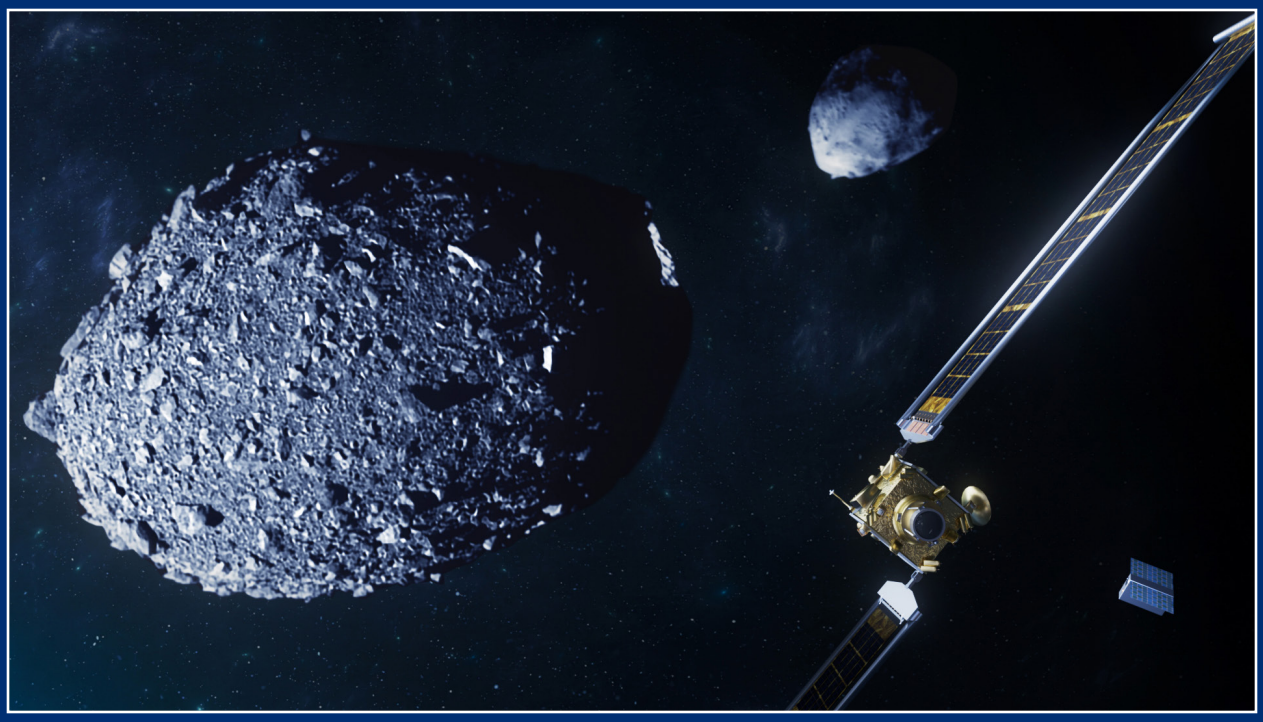

Final Technical Report
to the
National Aeronautics and Space Administration
for the
Double Asteroid Redirection Test (DART) Mission
October 2023

Elena Adams, DART Mission Systems Engineer
Johns Hopkins University Applied Physics Laboratory, Laurel, MD 20723 USA

Nancy Chabot, DART Investigation Team Coordination Lead
Johns Hopkins University Applied Physics Laboratory, Laurel, MD 20723 USA

Andrew Cheng, DART Investigation Team Lead
Johns Hopkins University Applied Physics Laboratory, Laurel, MD 20723 USA

Andrew Rivkin, DART Investigation Team Lead
Johns Hopkins University Applied Physics Laboratory, Laurel, MD 20723 USA

Edward Reynolds, DART Project Manager
Johns Hopkins University Applied Physics Laboratory, Laurel, MD 20723 USA

Caitlin Shearer, DART Project Manager
Johns Hopkins University Applied Physics Laboratory, Laurel, MD 20723 USA

Table of Contents

Executive summary

NASA's Double Asteroid Redirection Test (DART) mission was humanity's first attempt to move a celestial body, demonstrating the capability to perform a kinetic impact on a planetary defense–relevant sized asteroid. DART was part of the international collaboration known as the Asteroid Impact & Deflection Assessment (AIDA), involving NASA, the European Space Agency (ESA), the Agenzia Spaziale Italiana (ASI), and scientists around the world. DART was a key step to demonstrating preparedness to respond to planetary defense scenarios, and it provides a crucial data point for likely outcomes.

Near-Earth objects (NEOs) greater than 140 m in size are of particular interest to planetary defense because they have the potential to cause significant damage if they were to impact Earth, and also because they are difficult to detect, with less than 50% of the predicted population discovered as of 2022 (National Academies Press, 2022). With an appropriately sized spacecraft and enough warning (typically many years to decades), a kinetic impact can slightly alter the orbit of an asteroid in a way that, over time, prevents the asteroid from colliding with Earth in the future. DART's target was Dimorphos, the smaller (~150-m-diameter) member of the binary asteroid system (65803) Didymos, which is a near-Earth, potentially hazardous, and well-characterized asteroid system. By simply observing changes to the system after impact and comparing them with a pre-impact reference, it was possible to use ground-based telescopes to observe the deflection in the orbit of Dimorphos after impact.

Developed and operated by the Johns Hopkins University Applied Physics Laboratory (APL), the mission entered formulation in 2015 after multiple years of concept development. The project was administered according to NPR 7120.5, with technical oversight and funding through the Planetary Missions Program Office (PMPO) at Marshall Space Flight Center (MSFC) and overall support as a directed mission from NASA's Planetary Defense Coordination Office (PDCO). The DART spacecraft hosted a singular payload, the Didymos Reconnaissance and Asteroid Camera for Optical navigation (DRACO), and a deployable CubeSat contributed by ASI named the Light Italian CubeSat for Imaging of Asteroids (LICIACube). On 11 September 2022, DART deployed LICIACube, which subsequently followed the DART spacecraft at a safe distance and observed the immediate aftermath of the DART impact. DART was designed to autonomously detect, navigate to, and impact Dimorphos. This autonomous design was chosen to maximize the probability of impact, since commanding from the ground could result in course corrections arriving too late. On the day of impact, 26 September 2022, the spacecraft's autonomous systems successfully detected and locked on to Dimorphos, impacting its surface within 2 m of the center of the illuminated figure (Jensenius et al., 2023). No human intervention was required for a successful impact, demonstrating that humanity possesses the technology to perform a kinetic impact.

Within 2 weeks of impact, it was clear that the orbit of Dimorphos had been significantly altered. On 11 October 2022, NASA Administrator Bill Nelson announced that the new orbital period of Dimorphos was shortened by approximately 32 ± 2 min, from 11 h and 55 min before impact to 11 h and 23 min after impact. With additional observations over the following months, the accuracy of this measurement improved to a –33.24 min ± 1.4 s orbital period change (Naidu et al., 2023; Scheirich et al., 2023), and Beta (β), the momentum transfer enhancement parameter, was reported to be 3.6 (Cheng et al., 2023). Subsequent studies examined the details of DART's impact site, modeled the impact event, investigated the ejecta produced, and analyzed the dynamics of the Didymos system. These combined results clearly demonstrate that the project met all Level 1 mission requirements.

1 DART's Level 1 requirements

The topic of planetary defense encompasses understanding the impact hazards posed by natural objects and the efforts undertaken to mitigate or manage these threats. While planetary defense activities have been undertaken for decades (National Academies Press, 2010; 2022), in particular searching for and tracking near-Earth asteroids, the Double Asteroid Redirection Test (DART) was the first spacecraft mission dedicated to demonstrating a potential mitigation approach. DART was designed to demonstrate asteroid deflection through a kinetic impactor technique, which had been previously recommended as the first priority for a space mission in the mitigation area (National Academies Press, 2010).

The DART mission was driven by the Level 1 requirements briefly explained below:

- **DART-1.** DART shall intercept the secondary member of the binary asteroid (65803) Didymos as a kinetic impactor spacecraft during its 2022 September–October close approach to Earth.

The selected target for the DART mission was always the secondary member of the binary (65803) Didymos system, since it was a well-characterized eclipsing binary, with the 150-m secondary member a relevant size for demonstrating the kinetic impactor technique, and it offered an approach <0.1 au to Earth in the fall of 2022 (Cheng et al., 2015; Rivkin et al., 2021). In 2020, the secondary member (previously referred to as Didymos B) was named Dimorphos, meaning "two forms" in Greek; the name was chosen to reflect that Dimorphos would be slightly altered by DART's planned kinetic impact and, hence, would have pre-impact and post-impact forms.

- **DART-2.** The DART impact on the secondary member of the Didymos system shall cause at least a 73-s change in the binary orbital period.

The requirement to cause at least a 73-s change in the binary orbital period was derived from requiring that, after 1 month, the orbit phase would have been changed by at least one-tenth of an orbit, to ensure that the ground-based telescopes would be able to confidently measure the new period (Rivkin et al., 2021). If DART impacted near the center of Dimorphos and the incident momentum from the DART spacecraft was simply transferred to Dimorphos in a completely inelastic collision with no further momentum enhancement, a binary orbital period reduction of roughly 7 min was expected (Cheng et al., 2018). However, dynamical models and analysis showed that the resulting binary orbital period change could be more than 40 min for the momentum enhancement factors indicated by the impact simulations (Meyer et al., 2021).

- **DART-3.** The DART project shall characterize the binary orbit with sufficient accuracy by obtaining ground-based observations of the Didymos system before and after spacecraft impact to measure the change in the binary orbital period to within 7.3 s (1σ confidence).

The required value of 7.3 s was derived from ensuring the post-impact orbital period was determined with an accuracy of at least 10%, even if only the minimum 73-s period change resulted from DART's impact (Rivkin et al., 2021).

- **DART-4A.** The DART project shall use the velocity change imparted to the target to obtain a measure of the momentum transfer enhancement parameter, referred to as "Beta" (β), using the best available estimate of the mass of Didymos B.

The momentum enhancement parameter, β, quantifies how the ejecta produced during a deflection attempt contributes to the momentum imparted to the target. In a perfectly inelastic collision, with zero ejecta momentum, $\beta = 1$ by definition. However, the ejecta produced during a deflection

attempt carries off momentum, effectively giving an extra push to the target and making $\beta > 1$. Impact simulations conducted in preparation for DART's kinetic impact test indicated that there could be considerable enhancement to the momentum transferred to Dimorphos because of the ejecta produced, depending on the material strength, impact conditions, and other properties of Dimorphos and DART's impact (Stickle et al., 2022).

- **DART-4B.** The DART project shall obtain data, in collaboration with ground-based observations and data from another spacecraft (if available), to constrain the location and surface characteristics of the spacecraft impact site and to allow the estimation of the dynamical changes in the Didymos system resulting from the DART impact and the coupling between the body rotation and the orbit.

DART-4B encompasses the resulting effects from DART's first-of-its-kind kinetic impact test and enables a wide range of contributions to DART's planetary defense investigation, including data from another spacecraft, "if available." In 2018, the Light Italian CubeSat for Imaging of Asteroids (LICIACube) was added to the DART mission as a secondary spacecraft. Contributed by ASI, LICIACube was a 6U CubeSat developed by Argotec under the scientific coordination of the Italian Istituto Nazionale di Astrofisica (INAF) (Dotto et al., 2021).

2 Mission elements

2.1 Spacecraft

The DART spacecraft was heavily influenced by the technology demonstration components of the mission, while maintaining an emphasis on a low-cost implementation. Unlike traditional planetary

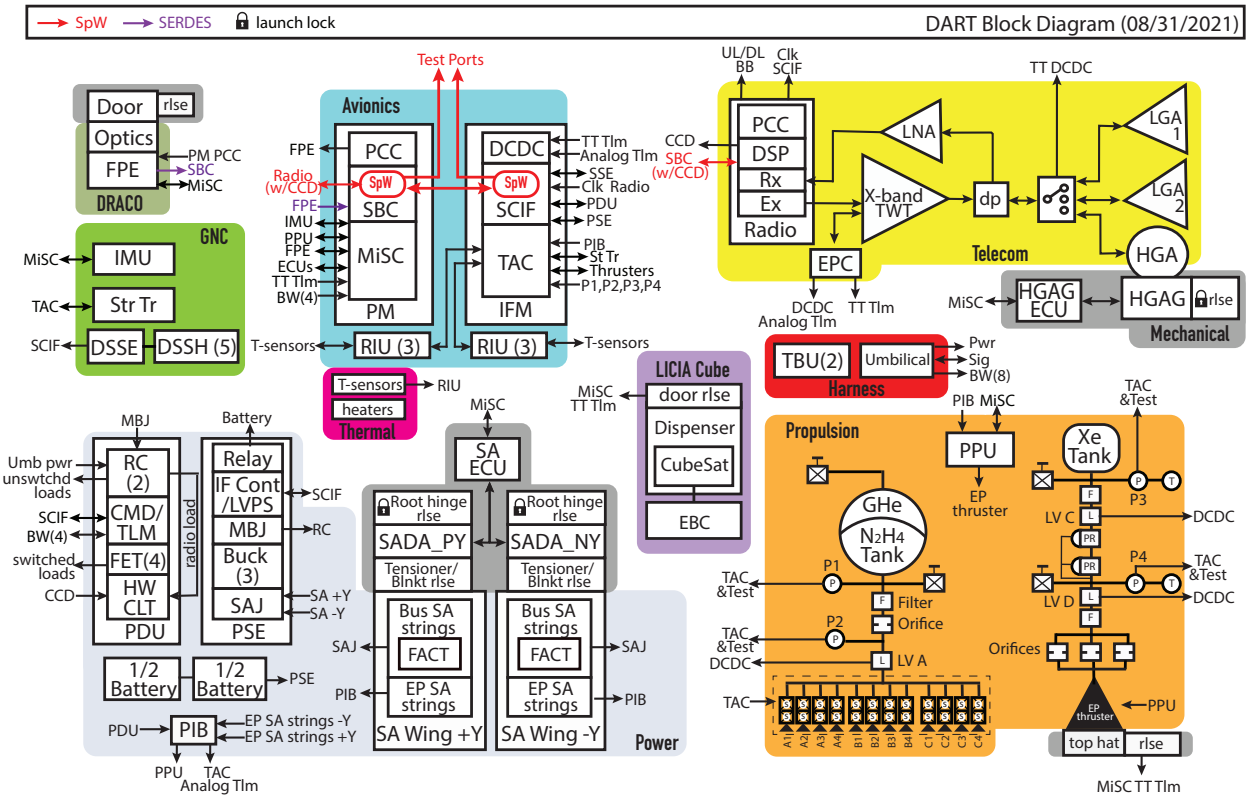

Figure 1. Spacecraft block diagram.

missions, DART was not mass constrained thanks to the flexibility in the launch window offered by low launch energy. DART's power consumption was driven by NASA's Evolutionary Xenon Thruster Commercial (NEXT-C) operational requirements. The high-rate imagery collected during the Terminal Phase of the mission determined the necessary downlink data rate and processing requirements. Pointing smear and jitter were driven by the DRACO Optical Navigation (OpNav) requirements during the arrival phase. Solar Array Drive Assembly (SADA) gimbals accommodated pointing of the Roll-Out Solar Arrays (ROSA) during the navigation to the asteroid. The NEXT-C gimbal, originally part of the design, was deliberately descoped in Phase C because of cost and schedule overruns. The high-gain antenna (HGA) gimbal allowed for the final terminal pointing orientation, with the solar array on the Sun, DRACO pointed at the asteroid, and the HGA pointed at Earth. Safe mode utilized the two low-gain antennas (LGAs) and a slow rotation around the NEXT-C-DRACO axis. Although the spacecraft had very limited redundancy, it was designed to be power cycled via a Hardware Command Loss Timer expiration in the Power Distribution Unit (PDU), similarly to how it was implemented on the Van Allen Probes. The spacecraft block diagram is shown in Figure 1. The mass and power margin trends through launch are shown in Figure 2 and Figure 3, respectively.

2.1.1 *Propulsion subsystem*

The DART spacecraft had two propulsion systems: a monopropellant liquid hydrazine system and an ion system using xenon propellant. The hydrazine propulsion system was the primary system that provided attitude control, ΔV for trajectory correction maneuvers (TCMs) for interplanetary transfer and final targeting, and Terminal-Phase divert maneuvers. It was a blowdown system with 12 Aerojet MR-103G thrusters. The ion propulsion system used the NASA NEXT-C engine at a single operating point at throttle level 28 and with ~3.5 kW of input power. At this setting, the engine provided 137 mN of thrust at 2943 s of specific impulse. NEXT-C was qualified to 6.9 kW of power, well above the DART design point. Likewise, the DART xenon tank had a capacity of ~140 kg of xenon at maximum pressure (2250 psi), which is well below the NEXT-C xenon throughput qualification of over 600 kg. The NEXT-C ion thruster was powered by the Power Processing Unit (PPU), which provided voltages required by various components of the thruster, and was controlled by spacecraft flight software (FSW). An extensive test campaign verified the FSW's ability to control and autonomously shut down the thruster and PPU in case of an issue (Badger et al., 2022).

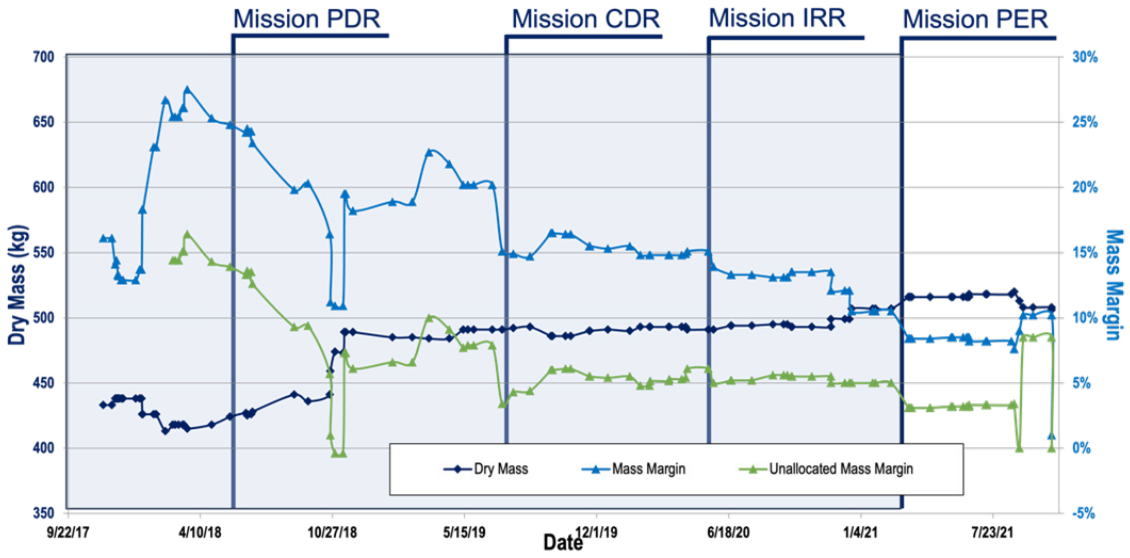

Figure 2. Spacecraft mass margin trends through launch. The total mass of the spacecraft at launch was 615 kg.

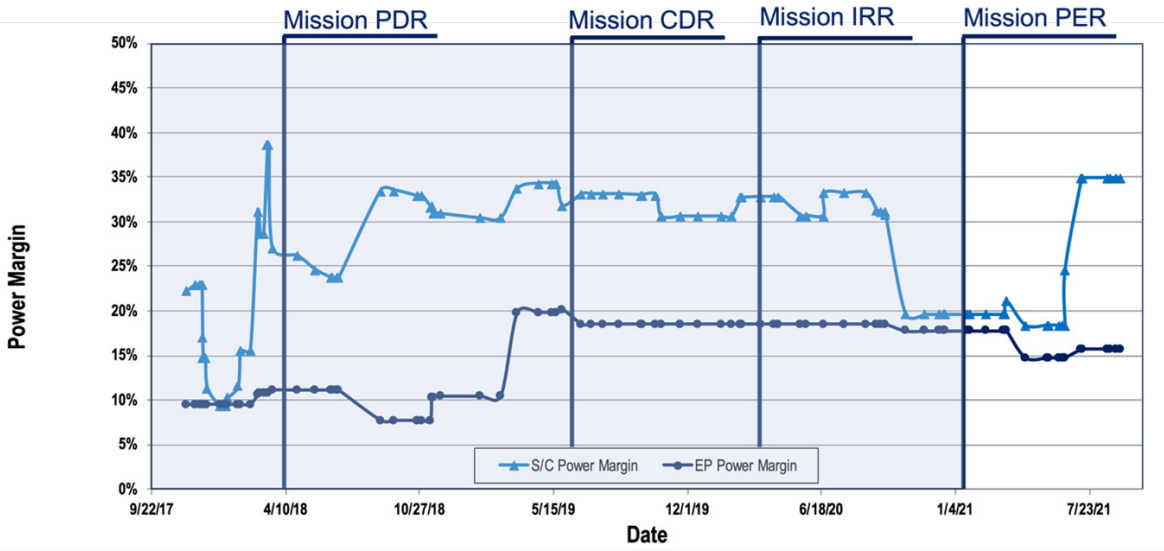

Figure 3. Spacecraft power margin trends through launch.

In Phase C, because of the launch vehicle selection and issues with NEXT-C timely development, the ion propulsion system was changed to be used for technology demonstration only instead of being the primary propulsion system. Before launch, NASA had agreed to the plan that DART would demonstrate the thruster via small maneuvers along the interplanetary trajectory for ~300 h of space operation. The 300-h estimate was lower than the original plan for NEXT-C, which required in-flight operation for 1000 h. However, the 1000 h relied on controlling the NEXT-C thrust vector to less than 1°, and as the mission developed, it was realized that the thrust vector measurements could not meet that requirement. In addition, the gimbal to control the NEXT-C thruster had to be descoped since it was not meeting programmatic milestones. The end-to-end full thruster system, including the PPU, could not be tested at the spacecraft level after integration and was accepted as part of the test-as-you-fly exceptions. At launch, the total hydrazine carried by DART was 50 kg, with a total dV99 of 55.2 m/s. Xenon propellant mass was 60 kg.

2.1.2 *Power subsystem*

The 22-m^2 ROSA provided the power for the spacecraft bus and NEXT-C engine. The solar arrays were electrically divided into two segments that powered the NEXT-C and the spacecraft bus independently. Each array was mounted to the spacecraft via a single-axis actuator. The total array area provided ~4 kW of power. The spacecraft power bus included an eight-series-cell lithium-ion battery implemented with GS Yuasa LSE 55 cells, physically split into two half-packs to accommodate spacecraft packaging. The plan was to use the battery during launch and to take up the transients in flight. The Power System Electronics (PSE) provided solar array regulation and limited battery charge. The PPU Interface Box bused together the high-voltage solar array strings and was designed to monitor the PPU current. It also housed the interface to the survival heaters for the PPU. The PDU provided switched power services to the rest of the spacecraft bus and enabled spacecraft power cycling.

Although the ROSA were not called out to be a technology demonstration in the DART Technology Development Plan and a prototype was officially demonstrated on the International Space Station (ISS) before DART, the team quickly discovered that a full demonstration, with flight cells and harness, presented a larger challenge than originally thought. Deployment uncertainties, together with the inability to perform fully g-negated flight testing at temperature, caused additional analysis burden for the guidance, navigation, and control (GNC) and

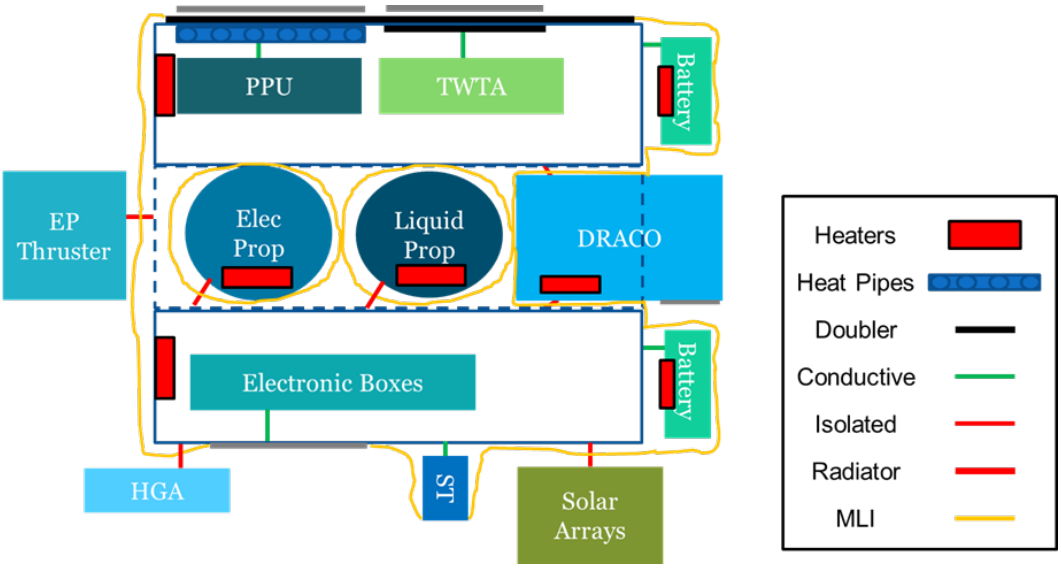

Figure 4. Thermal block diagram.

mechanical subsystems. In addition, the foam on the back of the arrays created particulates that endangered the DRACO measurements, creating additional burden for the contamination control team. The DART arrays had to be deployed autonomously (whereas the prototype arrays at ISS were deployed by astronauts), with redundant actuation of all of the devices. Late in the mission but before launch, a concern arose that deploying the arrays could cause the root hinge preload to be exceeded during deployment and movement of the spacecraft. The DART team worked with the NASA Engineering and Safety Center (NESC) to perform additional analysis to show that there was minimal chance that deployment would cause an issue on the spacecraft. DART launched with this risk open.

2.1.3 *Thermal subsystem*

The thermal subsystem was designed to be driven by the substantial NEXT-C PPU power dissipation and needed to accommodate eclipse at launch (which required the PPU to be preheated at the launch pad). The design included multilayer insulation blankets and white-painted radiator panels located on +Y and –Y panels. Figure 4 shows the thermal block diagram. Constant conduction heat pipes and a doubler transferred the heat from the PPU to the radiators. Heaters kept all of the components above their survival and operational temperature limits. Originally the heaters were designed to be mostly thermostatically controlled, except for DRACO, which had to control the detector to a small temperature range. However, after launch, additional autonomy rules were added so that more heaters could be turned on and off to mitigate challenges with the star tracker noise.

2.1.4 *Mechanical subsystem*

The spacecraft mechanical structure accommodated two propulsion systems, the large solar arrays, and the DRACO telescope. The structure was sized to withstand the launch loads for a variety of launch vehicles, as the structure fabrication led the launch vehicle selection. The structure featured a core cylinder, with multiple quadrant mid-deck panels and multiple closeout panels with little unsupported area. Figure 5 shows the mechanical layout. Early coupled loads analyses were performed to understand whether a SoftRide was required to reduce the launch loads. Once the launch vehicle was selected, the team implemented a Moog isolation system to meet the shock requirements.

One of the major considerations in the DART structure design was the ease of integration and test (I&T) at the spacecraft level. The core cylinder hosted the two propulsion tanks and allowed the propulsion

to be separately integrated into the primary structure. Most of the spacecraft boxes were placed on the +Y and –Y panels, which allowed for separate integration of these panels before the spacecraft was closed up. The top and bottom decks, with their associated components, completed the integration. It was extremely fortunate that DART implemented this approach, because the COVID-19 pandemic hit right as DART was about to start system integration. The separability of the various panels allowed Aerojet Rocketdyne (the propulsion provider) to finish integrating the propulsion system even in the COVID hot spot at Redmond, Washington, while the spacecraft panels with in-house components were integrated at the Johns Hopkins University Applied Physics Laboratory (APL) without compromising the schedule. The NEXT-C thruster and PPU were delivered to APL directly.

Figure 5. DART mechanical layout. The Radial Line Slot Array (RLSA), the solar array, and the radiator panel are clearly shown.

DART had many mechanisms to enable simultaneous satisfaction of multiple pointing objectives. The HGA and solar arrays were each mounted on single-axis gimbals. The solar arrays were deployed by a series of Frangibolt releases, and the HGA was locked at launch and deployed after the launch sequence was complete. The top hat covering the NEXT-C was deployed a couple of days later, before the start of the NEXT-C commissioning.

2.1.5 *Avionics subsystem*

The avionics subsystem used Parker Solar Probe spare boards to build up the interface module (IFM), with existing field-programmable gate array (FPGA) programming and FSW. The IFM had a SpaceWire router and provided command and telemetry for the PSE, the PDU, and the guidance and control (G&C) sensors other than the inertial measurement unit (IMU), as well as control for the hydrazine thrusters. It also took in pressure transducer, analog, and telltale telemetry across the spacecraft. The IFM hosted the spacecraft master clock, which was synchronized to the oscillator in the radio. It communicated with the Parker Solar Probe spare remote interface unit (RIU) strings, which provided temperature sensing.

The avionics processor module (PM) hosted imager and spacecraft processing in an RTG4 FPGA and Small-body Maneuvering Autonomous Real Time Navigation (SMART Nav) targeting and guidance in a UT700 LEON3FT processor. The imager data was received through a high-speed serializer/deserializer (SERDES) data link with DRACO, and command and telemetry were sent over serial interfaces to DRACO, the PPU, and the IMU. The PM also sent the gimbal commands and received analog telemetry from gimbal potentiometers. DRACO data was processed (windowed, binned, etc.), multiplexed together

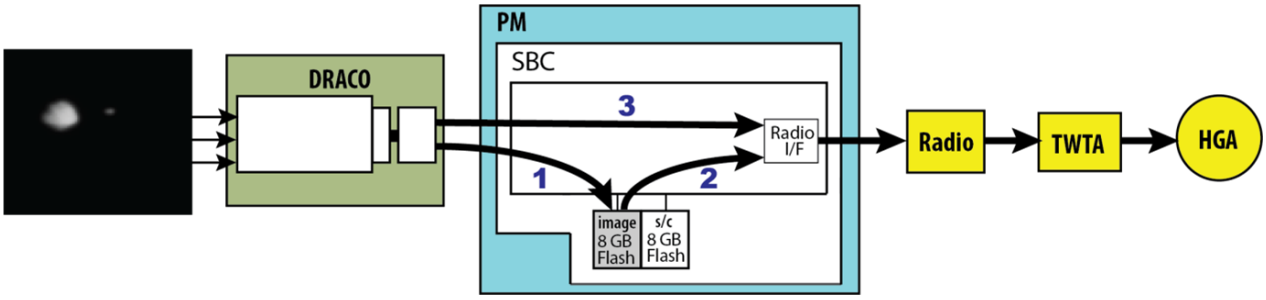

Figure 6. Data flow overview. Limited options were implemented to simplify managing the high-rate data. (1) Image data storage to flash (e.g., OpNavs); (2) flash to radio (transmitting OpNavs); and (3) sub-windowed images to radio in real time (terminal).

with engineering telemetry, and sent over SpaceWire link to the radio. The RTG4 FPGA in the PM was one of the components matured from technology readiness level (TRL) 4 to TRL 6 as part of the Preliminary Design Review (PDR) preparation, along with SMART Nav. Figure 6 shows the data flow from the point of acquiring DRACO images to downlinking data to Earth.

2.1.6 *Flight software*

DART FSW continued to build on the APL heritage code base using Goddard's Core Flight Executive (cFE) software framework, reusing ~60% of the command and data handling (C&DH) code and 100% of the autonomy engine code (Figure 7). Such extensive code reuse kept the software development affordable despite numerous new applications to control NEXT-C, DRACO, image-processing firmware, and SMART Nav. cFE's Operating System Abstraction Layer (OSAL) and publish-subscribe software bus facilitated an object-oriented approach to building new applications in a platform-agnostic fashion. Leveraging cFE's flexibility, the DART team developed a software-in-the-loop (SWIL) simulator allowing any laptop to run an emulation of the spacecraft for software development. This simulator

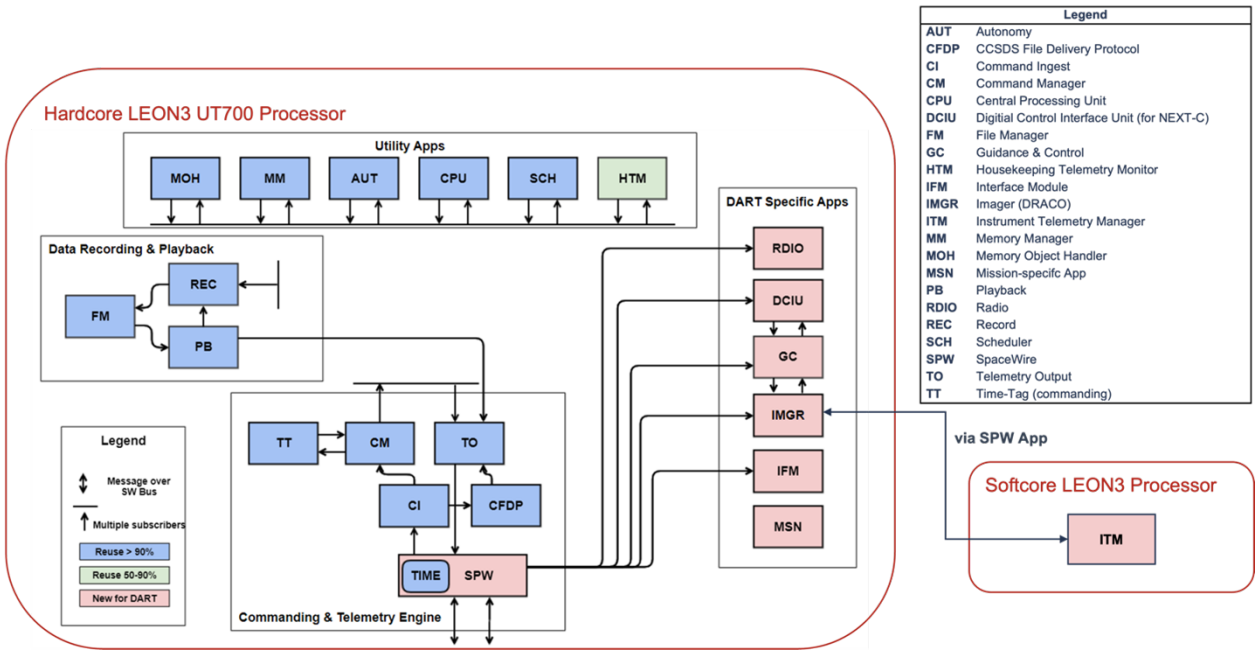

Figure 7. FSW diagram showing the application reuse for DART.

was used in early hardware testing of the NEXT-C, FSW deployment, test bed software, and a ground system that ran the thruster with the actual control FSW algorithm (and not a surrogate). The SWIL simulator not only provided a development environment for each developer but also doubled as a test suite, running regression tests any time code was changed (Heistand et al., 2019). Acceptance testing and a "small i" verification and validation approach, with a small independent team verifying the software as part of DART, resulted in a well-tested software suite.

Multiple versions of the software were released before integration, and only a few issues were found during system I&T. No post-launch software load was required, although a risk, with associated dollars, was carried at the project level. The success of the FSW can be traced to extensive prototype testing early in the program (Smith et al., 2020) and a small and dedicated team.

2.1.7 *Autonomy subsystem*

The DART FSW provided a "Monitor → Response" style autonomy engine, where the autonomy system was a collection of autonomy rules, macros, computed telemetry, and storage variables (Figure 8). It housed predefined sequences, such as launch and demotion into safe mode, and monitored the health state of all of the subsystems, while performing heater maintenance for DRACO and propulsion tanks. Accommodating the LICIACube CubeSat necessitated additional autonomy rules to ensure that its battery could do no harm to the spacecraft in cruise.

2.1.8 *GNC subsystem*

The DART GNC subsystem provided three-axis attitude control, executed the planned trajectory through the use of the dual-mode propulsion system, and pointed DART's articulated devices (solar arrays and HGA). Attitude estimation was accomplished through the use of a star tracker and IMU, with five Sun sensors providing Sun-direction information for safe mode. The GNC system implemented attitude control and TCMs via 12 hydrazine thrusters. For the NEXT-C demonstration, the GNC system achieved the necessary trajectory by pointing the thruster in the desired inertial direction via changes in the spacecraft attitude. The GNC system was also responsible for precision pointing the DRACO instrument to obtain optical navigation imagery in the 60 days leading up to the Didymos encounter. These images drove the control performance, as the large solar arrays paired with thruster control created challenging jitter and smear conditions when using the DRACO telescope. The GNC

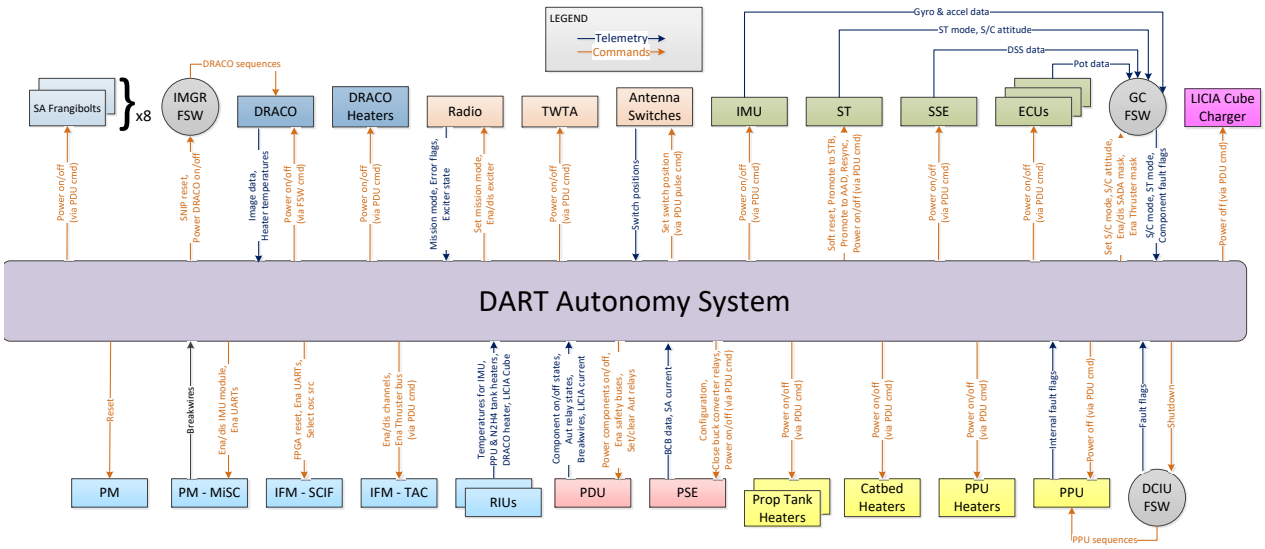

Figure 8. Autonomy context diagram.

system provided asteroid acquisition and tracking throughout the Terminal Phase and autonomously guided DART onto an impact trajectory with Didymos B; these functions were all provided via the SMART Nav system.

A principal challenge that DART faced was providing the navigation accuracy needed to ensure impact with the Didymos secondary. With a closing velocity of 6 km/s, navigating the spacecraft to a hypervelocity impact with an asteroid that is ~160 m in diameter required an onboard, autonomous approach, since the long communication latency with the ground meant that the mission's Level 1 impact requirement could not be met with ground-based commanding. Furthermore, telemetering full-resolution images to the ground in real time presented substantial challenges to the communication design, increasing mission cost and risk. To avoid the communication system complexity and latency associated with ground-based navigation, DART used the SMART Nav system to achieve impact with Dimorphos. SMART Nav was a collection of algorithms, firmware, and software used to identify and target the asteroid and then guide the spacecraft to impact. This system was developed as part of an Independent Research and Development effort in collaboration with APL's Air and Missile Defense Sector.

SMART Nav was divided into five functions: blobbing, centroiding, targeting, guidance, and divert maneuver commanding. Blobbing, an image-processing task running on an RTG4 FPGA, took raw images from DRACO and identified contiguous groups of illuminated pixels. The centroiding function, which also ran in the FPGA, identified parameters for each of the pixel blobs, including the centroid location, brightness, and size. The resultant table of pixel blob information was passed into the targeting software running on a LEON3 processor. Targeting maintained a history of blob parameters and, by coupling this information with information about vehicle attitude, identified and tracked the asteroid (nominally, the brightest and/or largest blob). Targeting provided the line-of-sight (LOS) measurement to the guidance software. The guidance filter ran as a part of the onboard G&C software, and as such, it had access to accurate attitude information to help resolve this LOS measurement into inertial coordinates. Using the principles of proportional navigation, the guidance software used an extended Kalman filter to predict the miss distance at closest approach as well as the miss distance uncertainty. These estimates of miss distance and uncertainty were provided to a maneuver command function inside the G&C software that maintained knowledge of onboard propellant and time to impact. Based on this information, the maneuver command function determined whether a ΔV maneuver had to be made to reduce the miss distance, and if so, computed the necessary ΔV command to be acted on by the maneuver control software.

Numerous challenges complicated SMART Nav design and implementation. To ensure the timely processing of images, a software implementation on a flight-qualified processor was not feasible; this necessitated that images be processed in an FPGA, complicating the avionics design. The image processing was further complicated because Dimorphos was not well characterized, leading to uncertainty on its surface reflectivity and shape properties. To ensure the impact footprint requirement was met, the shadowed side of the asteroid had to be distinguished from the background, and this had to be done in the presence of the parametric uncertainty of the asteroid. Another issue for the targeting software was the transition from tracking the primary asteroid to tracking the secondary. This transition was expected to occur roughly 60–90 min before impact and had to be managed without ground assistance. The difficulty was that the transition could have been affected by the asteroid parameters mentioned above, the secondary's orbit, rotation, and image characteristics such as jitter and smear. Additionally, it was not known for certain that the asteroid system was binary; there could have been a second moon that had to be handled by the targeting algorithms. The guidance filter used linearized models of asteroid motion to maintain mathematical simplicity and robustness. This model could cause substantial motion of the target in the minutes before impact owing to

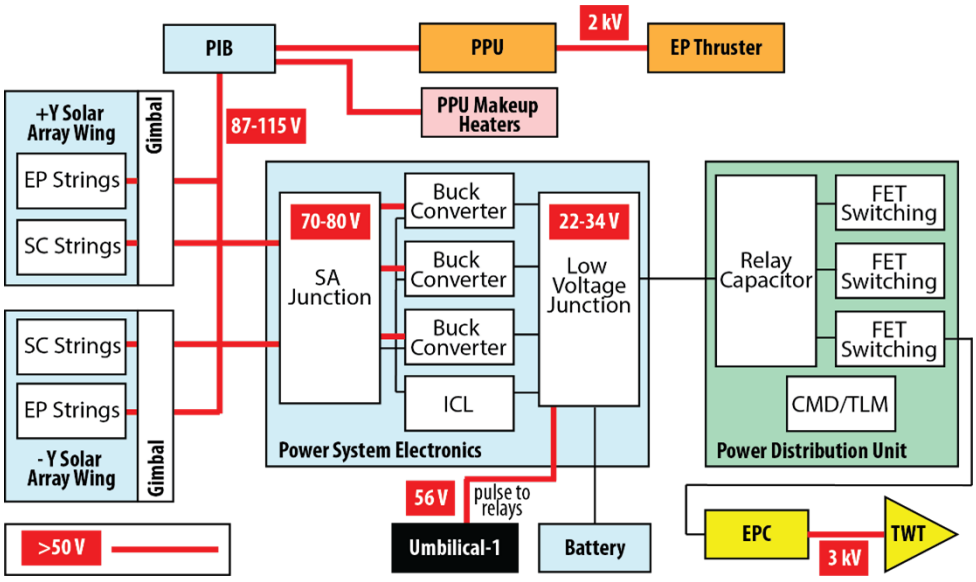

Figure 9. The high-voltage block diagram, showing where the harness subsystem used double insulation and other protections, including heightened awareness, in test.

secondary acceleration with respect to the primary, asteroid rotation, and lighting conditions resulting in apparent motion. This resulted in guidance maneuvers up until a few minutes before impact to ensure that the center-of-figure impact requirement was met. Finally, with the large closing velocity, the spacecraft and SMART Nav system had to remain fully functional until the final few seconds before impact because only the last few images would meet the Level 1 resolution requirements.

2.1.9 *Communications subsystem*

DART communicated in X-band with the Deep Space Network (DSN) using two LGAs and one HGA. The two LGAs provided nearly spherical coverage. The HGA was an RLSA and was used for planned downlinks and impact phases. It was mounted on a single-axis gimbal with a ±25° range of motion. The radio was a rebuild of the Parker Solar Probe radio without the Ka-band slice. It supported a variety of uplink and downlink rates, most importantly a 3-Mbps downlink rate during terminal approach. The traveling-wave tube amplifier (TWTA) was a requalified unit from Solar Terrestrial Relations Observatory (STEREO), providing 65 W of RF power. The HGA RLSA was part of the technology maturation for the DART mission and demonstrated TRL 6 at the PDR.

2.1.10 *Harness subsystem*

The harness subsystem included box-to-box wiring, flight arm plugs and ground straps, and connectors and special ground-support-equipment cables for testing in system I&T. It accommodated standard voltage and signal routes, as well as SpaceWire, and high-voltage power (Figure 9), with an estimate of ~3500 wires at the Pre-Environmental Review (PER). The harness was built up on a DART spacecraft mock-up and tested to ensure continuity and pin retention.

2.2 Payload

2.2.1 *DRACO*

DART flew the Didymos Reconnaissance and Asteroid Camera for Optical navigation (DRACO) narrow-angle telescope, designed to obtain optical navigation images of Didymos for ground navigation and to target Didymos/Dimorphos in the Terminal Phase. The telescope also obtained images of the impact site before DART impact. DRACO telescope parameters are shown in Table 1, and a block diagram is shown in Figure 10. DRACO is fully described in Fletcher et al. (2018).

Table 1. DRACO instrument characteristics.

Characteristic	Measurement
Aperture	208 nm
F number	f/12.6
Wavelength	400–1000 nm
Field of view (FOV)	0.29° full angle
Instantaneous FOV (IFOV)	2.5 µrad, 4.9 µrad (binned)
Pixel sample distance (PSD)* (300 km)	1.0 m
PSD* (150 km)	0.5 m
PSD* (30 km)	0.1 m
Signal-to-noise ratio (SNR) (30 days)	>7
SNR (final)	>100

DRACO consisted of a telescope, including a cover, connected to a BAE Systems' complementary metal oxide semiconductor (CMOS) image sensor. To minimize the latency in data acquisition and transmission, the data was read out by the focal plane electronics (FPE), which sent data to the single-board computer (SBC) in the PM. DRACO had firmware and software running as part of the SBC.

The optical design of the telescope was based on the New Horizons Long Range Reconnaissance Imager (LORRI), consisting of a composite ZERODUR Ritchey–Chrétien telescope with a field-flattening lens group before the detector. The main metering structure surrounded the primary mirror with legs for both the secondary mirror mount and the detector mount. This metering structure was attached to the spacecraft via thermally isolating flexures.

The FPE provided voltage regulators, clocks, and commands to the BAE CIS2521 CMOS sensor. The CIS2521 had a 5T pixel, low read noise (2e-) and a 2560 × 2160, 6.5-µm pixel architecture. The CIS2521 read out two simultaneous gain states (high and low) with 11 bits of data. The FPE combined these two 11-bit data streams into a single 16-bit data stream inside its RTAX2000 FPGA and then sent the image data to the PM SBC via a SERDES interface.

Detector-level characterization measured dark current, gain, quantum efficiency, and full-well and read noise. Dark current was negligible at the –20°C operating temperature, and read noise was

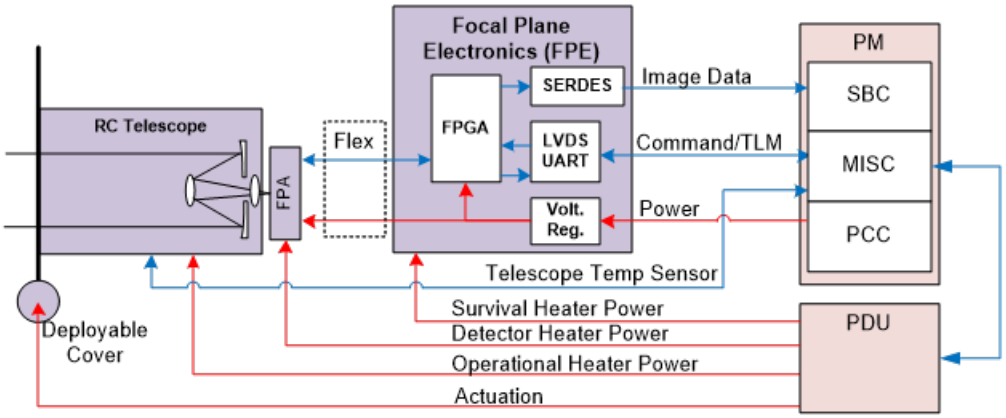

Figure 10. DRACO block diagram.

<2e- for 30× gain mode. Additional radiation testing qualified the detector and readout electronics to the space environment (Fletcher et al., 2022).

During development, DRACO's engineering model telescope experienced a vibration failure that resulted in the late redesign of the mounting of DRACO's primary mirror. The DART spacecraft went through the observatory thermal vacuum/balance campaign with an engineering model of the FPE, and without a DRACO telescope, while the new mounting scheme for the flight DRACO was being developed. The DRACO telescope was successfully integrated onto the DART spacecraft in June 2021 and went through the observatory structural campaign (vibe, shock, deployments) in July 2021. Limited confirmation of optical performance was executed after the structural campaign. To prevent contamination of the DRACO telescope, the instrument had a one-time cover that was actuated in flight and kept on mostly continuous purge during I&T.

2.2.2 *LICIACube CubeSat*

To observe the impact and resulting ejecta plume in situ, DART carried a CubeSat provided by the Agenzia Spaziale Italiana (ASI). The Light Italian CubeSat for Imaging of Asteroids (LICIACube) was a 6U+ CubeSat designed, built, and operated by Argotec. LICIACube largely mirrored the ArgoMoon CubeSat flown as a part of the Artemis 1 mission. The CubeSat mission posed a substantial challenge, as it required enormous capability in a 6U form factor. The CubeSat carried LEIA, a narrow-FOV camera, and LUKE, a wide-FOV imager with a red, green, blue (RGB) Bayer pattern filter (Dotto et al., 2021), as shown in Figure 11. Some key features of the CubeSat design included a dual-mode propulsion system, an autonomous system to acquire and track the asteroid throughout the encounter, and an X-band communication system to telemeter encounter imagery to Earth. LICIACube was carried to the

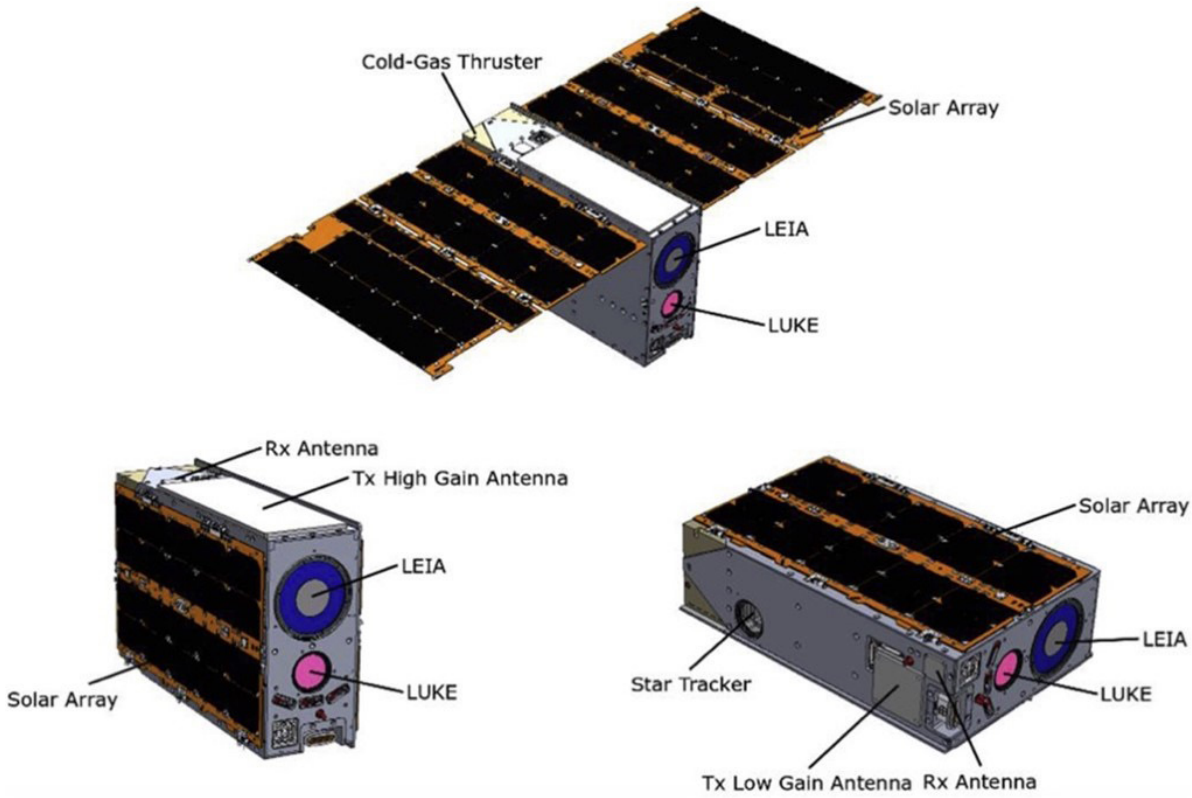

Figure 11. Layout of the LICIACube CubeSat (Dotto et al., 2021).

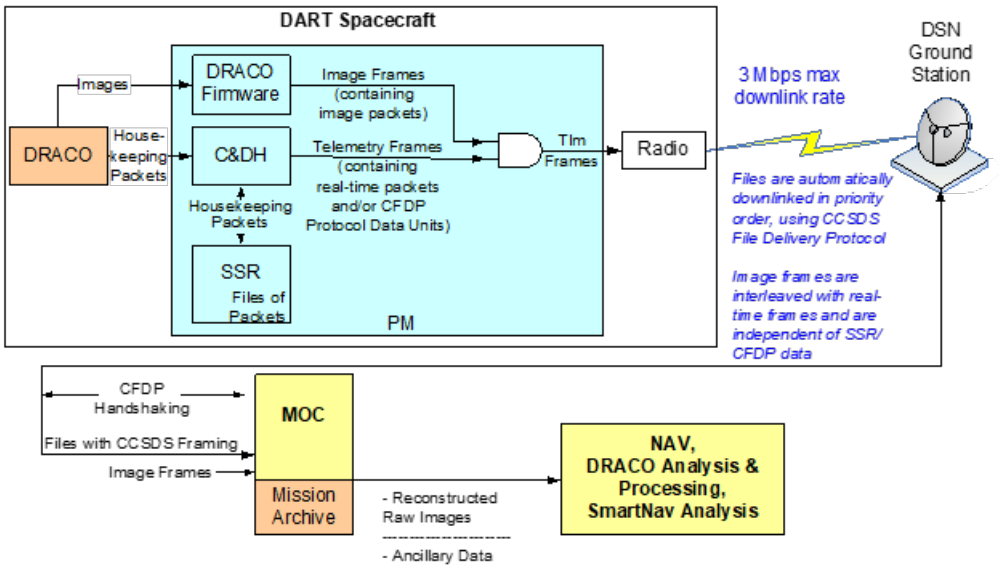

Figure 12. Ground system architecture. The MOC was located at APL

Didymos system by DART, and it was to be deployed 10 days before Didymos impact. The CubeSat relied on its onboard propulsion systems to alter its trajectory, introducing sufficient lag in the arrival time but providing LICIACube an opportunity to image the DART spacecraft impact, resultant ejecta plume, impact crater, and departure hemisphere of both Didymos and Dimorphos. LICIACube was accommodated on the DART spacecraft via a canisterized satellite dispenser (CSD), and its battery temperatures were monitored throughout I&T and cruise.

2.3 Ground segment

The DART ground segment consisted of the Mission Operations Center (MOC) and the ground system hardware and software that resided in the MOC and the I&T facility. It also included the ground stations used to communicate with the spacecraft after launch. Also supporting post-launch operations were the navigation, mission design, and GNC teams, as well as the spacecraft and DRACO engineering teams. A diagram showing DART ground architecture facilities and functions and the associated data flow is shown in Figure 12.

2.4 Launch vehicle

The DART mission was originally designed to be a secondary payload on a rideshare as a commercial procurement, with a Class D risk posture. However, as the development progressed, and as the requirements for the mission became clear, the launch services provider (LSP) was asked to take on a launch vehicle contract, and the provider selected a SpaceX Falcon 9 as the launch vehicle with DART as a primary payload.

3 Mission operations and DART impact results

The DART spacecraft was launched from Vandenberg Space Force Base on 24 November 2021, 06:21 UTC, on the SpaceX Falcon 9 launch vehicle. After separation, the spacecraft detumbled and established contact via DSN autonomously. The ROSA autonomously deployed successfully within hours after launch, the star tracker was turned on, and the spacecraft was reconfigured for cruise. It then followed the trajectory (Figure 13) developed by the mission design and navigation teams for

10 months before encountering the Didymos system. The spacecraft was tracked from the ground radiometrically and via Delta DOR.

The mission timeline is shown in Figure 14. The first 30 days after launch were devoted to commissioning. The high-gain launch lock was released, and the high-gain gimbal was actuated to characterize the HGA. The DRACO door was opened, and the NEXT-C cover (top hat) was released. The IMU, star tracker, and Sun sensor were calibrated. DRACO's performance was characterized, and DRACO was calibrated in flight. The spacecraft completed all subsystem commissioning and characterization successfully. After the xenon propulsion system was commissioned, NEXT-C was briefly demonstrated, but an observed anomaly in the spacecraft's PSE (John et al., 2023) prevented its further use. As part of the mitigation of that anomaly, the spacecraft was not allowed to off-point the solar arrays from the Sun, lest it would trigger a change in the state of the power system, which prevented full demonstration of the Transformational Solar Array, the concentrator cells on ROSA. The spacecraft autonomy was updated to implement changes to the system to ensure safe operation. The spacecraft team also adjusted the G&C algorithms to stabilize the solar arrays.

After launch lock deployment, the RLSA antenna was routinely used to downlink data and rehearse the Terminal Phase. Along the way, the team calibrated DRACO and SMART Nav, rehearsed the encounter and the Terminal Phase, and demonstrated new technologies. The CORE Small Avionics

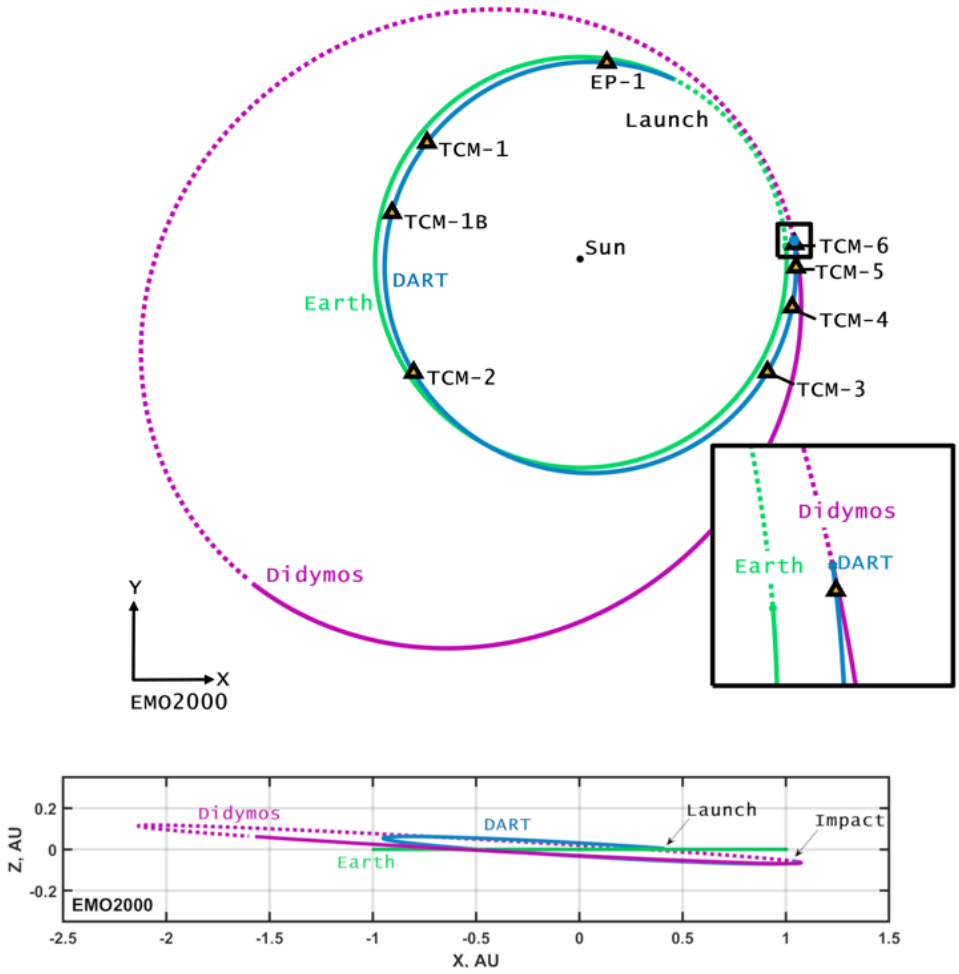

Figure 13. The final trajectory for the DART spacecraft.

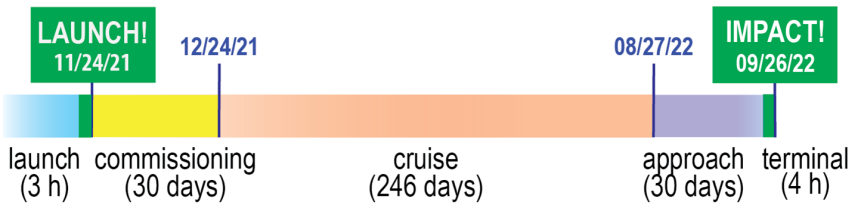

Figure 14. Mission timeline.

suiTe (CORESAT) operated the spacecraft as intended and exercised the SMART Nav algorithms during rehearsals and special calibration tests, such as observing Jovian moons. To stay on course, six TCMs were performed. Timing was characterized to ensure 3-Mbps downlink with low latency so that the images were on the ground within <10 s of being acquired and multiple streams came into the MOC.

Even before DART launched, the project was concerned about the star tracker's operation in flight—particularly whether the small changes in the star tracker noise (e.g., stars coming in and out of the edges of the star tracker's FOV) would impact the ability to guide the spacecraft into Dimorphos. To address the star tracker noise, a late tracker bracket was redesigned to further align the star tracker and DRACO instrument. In addition, the team devised a number of in-flight tests to ensure understanding of system performance, including the influence of flexing the solar arrays in the terminal spacecraft attitude and performance of the IMU. The team also worked on minimizing any movement on the spacecraft that could alter the alignment of DRACO and the star tracker, locking the HGA and solar array gimbals in a preferred orientation. The team performed extensive image streaming exercises to tease out the effects of star tracker noise and then fed the results back into Monte Carlo simulations to confirm SMART Nav performance. One of those simulations revealed that the spacecraft panels were flexing because of heater power cycling, and this discovery caused the team to replan the last month of operations. As a result, the autonomy was updated to cycle the heaters at a higher rate to lower the amplitude of temperature cycling and to reduce the cyclical misalignment of DRACO to the star tracker. In addition, LICIACube was deployed 5 days earlier than the pre-launch schedule called for. This provided enough time to perform additional tests for star tracker noise after deployment and to confirm a successful fix to the star tracker noise just in time for the day of impact.

The team performed seven TCMs over 10 months. The first maneuver turned on the NEXT-C thruster and operated it for 2 h. TCM-1 was split into TCM-1A and TCM-1B because of what was interpreted to be an anomalous power draw of the battery during the first TCM-1A. TCM-4 through TCM-6 placed DART on a favorable trajectory to Didymos, with the final maneuver shifting the B-plane by ~3.5 km. Subsequent tracking indicated that the post-maneuver error was 0.21 × 0.06 km 3σ and within the expected body of Didymos (meaning that the spacecraft would likely impact Didymos if no subsequent maneuvers were conducted) (Bellerose et al., 2023; Atchison et al., 2023).

In addition to all of the in-flight tests, the team rehearsed the Terminal Phase many times in the MOC. These rehearsals included conducting closed-loop simulations of nominal and faulted Terminal Phases, planning and testing the 21 terminal-phase contingencies, practicing execution in real time, and simulating the last 24 h before the Terminal Phase. The team also practiced LICIACube release and contingency operations. In preparation for the Terminal Phase, the team completed a rigorous cycle of reviews that covered subsystem operations and performance and mission operations, ground, and DSN/ESTRACK readiness. The cycle culminated with a Critical Event Readiness Review (CERR) that demonstrated the team's preparedness for the Terminal Phase. There was only one chance for

this phase to work. Ultimately, no contingencies had to be executed in the Terminal Phase, and the impact was successful.

3.1 Achievement of the Level 1 requirements

The following sections document the achievement of DART's Level 1 requirements. The full text for each requirement is stated in section 1 of this report.

3.1.1 *DART-1: Impact Dimorphos*

DART successfully impacted the asteroid Dimorphos on 26 September 2022, becoming the first mission to demonstrate asteroid deflection (Daly, Ernst, Barnouin et al., 2023a). Over a million concurrent viewers around the world watched live via a NASA broadcast as the DART spacecraft streamed images to Earth up to the final sub-second before its impact with Dimorphos.

Telescopic observations obtained through January 2021 were used to calculate Dimorphos' orbit and were delivered to the project in February 2021. This orbit was calculated to sufficient accuracy to predict Dimorphos' orbital phase to within 6.6° (3σ) at the time of impact, which enabled some operational planning to occur earlier than expected.

DRACO (Fletcher et al., 2022) first detected the Didymos system 61 days before impact. Optical navigation was used heavily during the final month to ensure the spacecraft was positioned to impact Dimorphos and to inform the associated TCMs (Rush et al., 2023; Bellerose et al., 2023). At 4 h and 5 min before impact, SMART Nav took control of the spacecraft navigation (Jensenius et al., 2023). The SMART Nav system obtained its final stable track for Dimorphos 68 min before impact, and 50 min before impact, SMART Nav began maneuvering toward Dimorphos. The DART spacecraft impacted Dimorphos on 26 September 2022 at 23:14:24 UTC, with a speed of 6.1 km/s and a mass of 579 kg (Daly, Ernst, Barnouin et al., 2023a). Figure 15 shows the milestones leading up to the impact with Dimorphos, from the time when SMART Nav began. Evaluation of DART's impact shows that the spacecraft impacted within 2 m of the center of the illuminated figure (Jensenius et al., 2023) and within 25 m of the center of figure of Dimorphos, with an impact angle of ~17° from the surface normal (Daly, Ernst, Barnouin et al. 2023a). Autonomously targeting a small asteroid with limited prior knowledge at high speed was a key accomplishment for the DART mission and marked the achievement of the DART-1 Level 1 requirement.

3.1.2 *DART-2: Change the binary orbital period*

After DART's kinetic impact, both photometric observations and planetary radar observations began, with the goal of determining the post-impact binary orbit period through two independent approaches. Although the ejecta produced by DART's impact immediately brightened the system for ~24 days (Graykowski et al., 2023; Kareta et al., 2023), the first photometric observations that could detect a mutual event in the light curve were obtained on 28 September 2022, just 29 h after DART's impact (Thomas et al., 2023a). The first radar detection of Dimorphos in the echo power spectra occurred even earlier, on 27 September, just 12 h after DART's impact (Thomas et al., 2023a). Radar observations continued through 13 October, during the time when the distance between Earth and the Didymos system made such observations possible; echo power spectra were obtained during each radar observing window, and range-Doppler images were acquired on 10 different days (Thomas et al., 2023a); examples are shown in Figure 16. The initial set of post-impact photometric observations extended through 10 October, until the bright Moon reduced the precision with which photometric observations could be obtained. During the time period from impact through 10 October, 25 mutual events were measured (Thomas et al., 2023a); examples are shown in Figure 17.

Independent analysis of both the photometric observations and the radar observations yielded the same determination of the binary orbital period change. During a NASA press conference on 11 October 2022, just 15 days after DART's impact, the NASA administrator announced the initial result from the DART team that the binary orbital period of Dimorphos had been reduced by 32 min with

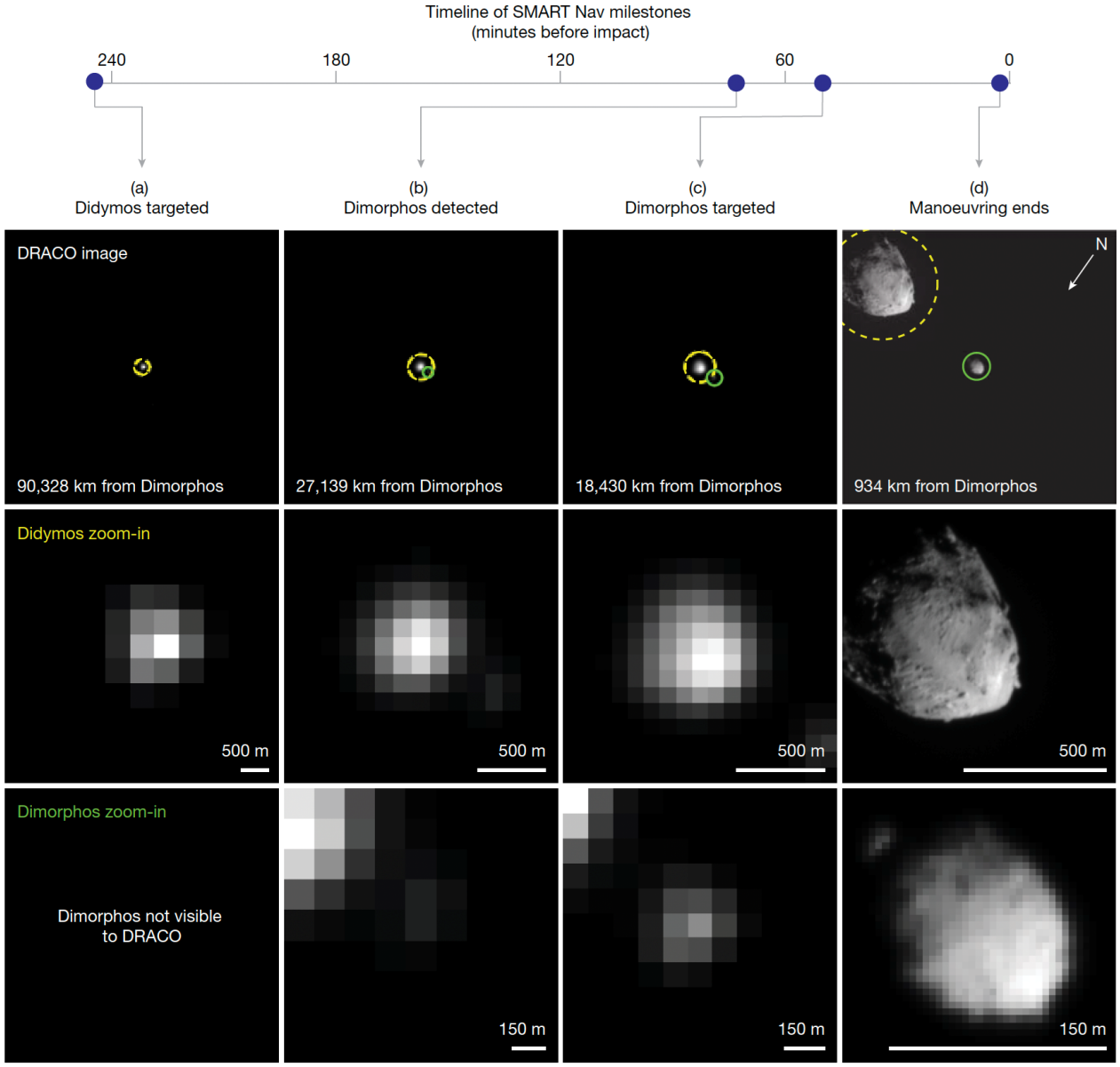

Figure 15. Milestones leading to the impact with Dimorphos from the time SMART Nav began targeting until the end of SMART Nav maneuvering. a–d, Each column corresponds to a milestone: Didymos targeted (a), Dimorphos detected (b), Dimorphos targeted (c), and end of maneuvering (d). Each row shows, from top to bottom, the raw DRACO image at the time of that milestone. In the top row, the circles indicate the two asteroids detected by onboard processing and identified by SMART Nav (the dashed yellow circles indicate Didymos, and the solid green circles indicate Dimorphos). The second row shows a zoomed-in image of Didymos, and the third row shows and a zoomed-in image of Dimorphos. The SMART Nav system used information in DRACO images to successfully impact Dimorphos. In all images, the north pole of Dimorphos (+Z) is toward the bottom left. From Daly, Ernst, Barnouin et al. (2023a).

an uncertainty of ±2 min. Continued analysis of these initial data over the next months refined the period change to −33.0 ± 1.0 (3σ) min (Thomas et al., 2023a). This result definitively verified that the DART-2 Level 1 requirement had been met, with the DART kinetic impact into Dimorphos producing at least a 73-s binary orbital period change.

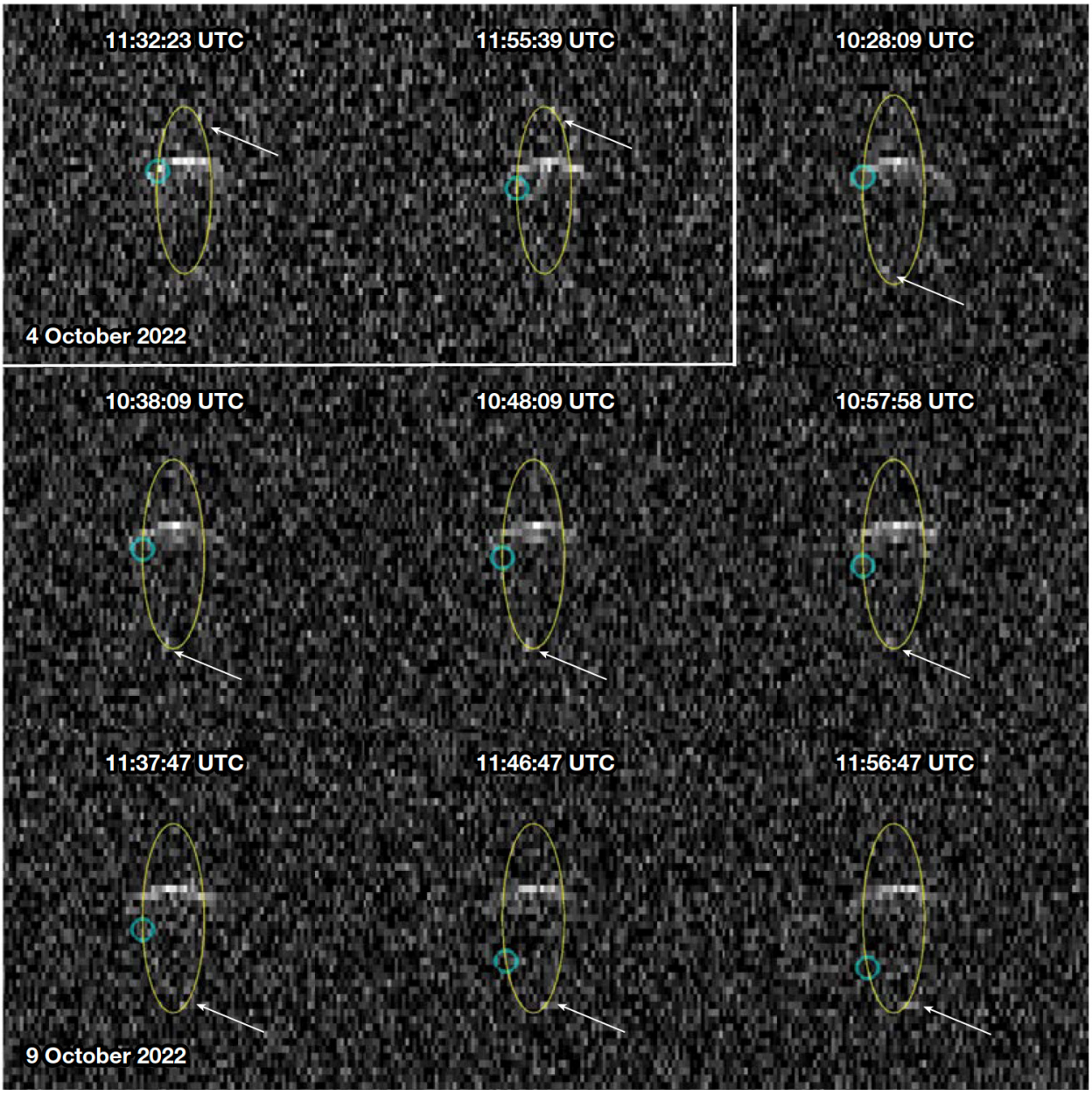

Figure 16. Radar range-Doppler images of the post-impact Didymos system. Radar range-Doppler images obtained on 4 October using Goldstone and on 9 October using Goldstone to transmit and the Green Bank Telescope to receive. In each image, the distance from Earth increases from top to bottom, and the Doppler frequency increases to the right, so rotation and orbital motion are anticlockwise. The broader echo is from Didymos, and the smaller, fainter echo shown by arrows is from Dimorphos. The green circles show Dimorphos positions predicted by the pre-impact orbit. The yellow ellipses show the trajectory of Dimorphos. From Thomas et al. (2023a).

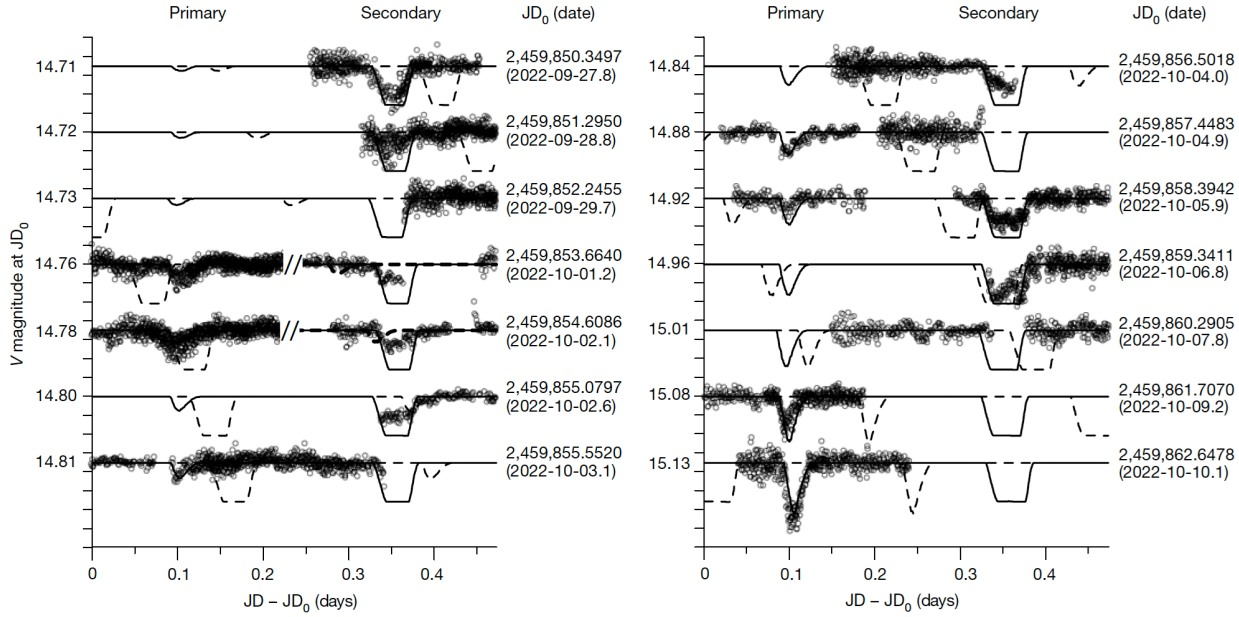

Figure 17. Observed mutual events of the Didymos system. The data are marked as circles, and the solid curve represents the synthetic light curve for the best-fit post-impact solution. The dashed curve is the pre-impact orbit prediction. The primary and secondary events are shown on the left and right sides of the plots, respectively. In some cases, the observations of a secondary event precede those of a primary event (that is, their order in the data set is the inverse of that shown in the plot). These events are presented in reverse order and are separated by a double-slash (//) symbol in the plot. From Thomas et al. (2023a).

3.1.3 *DART-3: Precisely measure the period change*

Photometric observations from 2015 to 2021 obtained by 11 telescopes were combined with data from observations obtained in 2003 to determine the pre-impact binary orbital period of Dimorphos about Didymos (Pravec et al., 2022). The pre-impact binary orbital period was determined with two separate analysis models, resulting in values of 11.921473 ± 0.000138 h (3σ) (Scheirich and Pravec, 2022) and 11.921487 ± 0.000028 h (1σ) (Naidu et al., 2022). Using additional pre-impact observations from 2022 (Moskovitz et al., 2023), the pre-impact binary orbital period was further refined to 11.921493 ± 0.000091 h (3σ) (Scheirich et al., 2023). These pre-impact best estimates are consistent with each other within their uncertainties, fulfilling a portion of the DART-3 Level 1 requirement to determine the binary orbital period precisely before impact. Additionally, this pre-impact knowledge put the team in a good position to be able to achieve the remainder of the DART-3 Level 1 requirement by using the post-impact observations to determine the change in the binary orbital period to within 7.3 s (1σ) without being limited by the pre-impact knowledge of the system.

Post-impact photometric observations were carried out for ~5 months, extending through February 2023. A total of 28 telescopes distributed across the globe acquired >38,000 individual exposures with a total time on sky of >1000 h (Moskovitz et al., 2023). This unprecedented observational data set of a binary asteroid system enabled a high-precision determination of the post-impact period change. By applying the same two independent analysis model approaches used before impact, the binary orbital period after all these observations was determined to be 11.3675 ± 0.0012 h (3σ) (Scheirich et al., 2023) and 11.3674 ± 0.0004 h (1σ) (Naidu et al., 2023), indicating a period change of –33.24 min or –32.25 min, respectively. The two independent analysis values provide the same result within their

uncertainties, with each reporting 1σ errors <2 s, which is well below 7.3 s and, thus, achieves the DART-3 Level 1 requirement.

The high quality of the post-impact observational data set additionally allowed an examination of whether the period change remained at a constant value during the time frame of the observations, from September 2022 through February 2023. The two analysis models indicate that the binary orbital period immediately after impact was ~20 to 30 s longer than the final period observed (Naidu et al., 2023; Scheirich et al., 2023). The changing period after DART's impact is consistent with the presence of an exponentially decaying drag-like force acting on Dimorphos, with an estimated time constant of ~12 days (Naidu et al., 2023). By a few months after DART's impact, the data do not indicate any further measurable change in the orbital period (Scheirich et al., 2023; Naidu et al., 2023). Dynamical models suggest that this evolution of the binary orbital period that followed DART's impact is consistent with outward scattering of ejecta from the system decreasing the orbital period, although more detailed modeling is warranted (Richardson et al., 2023).

The extensive post-impact observational data sets also contributed key insights into understanding DART's impact event and the dynamics of the binary Didymos system. These aspects are discussed in section 3.1.5. It is worth noting here, though, that it is necessary to account for the rotation of Didymos in the light curve analysis to determine the binary orbital period. The analysis shows that the rotation period of Didymos after impact is indistinguishable from its pre-impact value of 2.260 ± 0.001 h (3σ) (Thomas et al., 2023a).

3.1.4 *DART-4A: Determine the momentum enhancement factor*

The mass, impact velocity, and incoming trajectory of the DART spacecraft are well-determined quantities (Daly, Ernst, Barnouin et al., 2023a), leaving the major unknown components required to determine β as the change in the orbital velocity of Dimorphos, the mass of Dimorphos, and the net ejecta direction. Appendix B of Rivkin et al. (2021) details the formulation of β and its application in the context of the DART mission. A Monte Carlo approach was used to produce a distribution of velocity changes that was consistent with the period change determined by the ground-based observations (Thomas et al., 2023a) and that accounted for uncertainties in the Didymos system parameters (Cheng et al., 2023a). The net ejecta direction was constrained using observations from the Hubble Space Telescope (HST) (Li et al., 2023) and LICIACube images (Dotto et al., 2023; Cheng et al., 2023a), which showed the net ejecta direction to be opposite of DART's incoming trajectory to within ~20° (Cheng et al., 2023a; Hirabayashi et al., 2023).

The sizes of Didymos and Dimorphos and their separation distance were constrained by DRACO approach images, and DRACO images were also used to determine the shape, and hence volume, of Dimorphos (Daly, Ernst, Barnouin et al., 2023a; Thomas et al., 2023a). The total mass of the binary system is constrained by the pre-impact orbit period, although given that Didymos is significantly larger than Dimorphos, this does not directly constrain the mass of Dimorphos. Telescopic spectral observations of the Didymos system taken after DART's impact, during the following days when the signal from the Didymos system was dominated by ejecta from Dimorphos, indicate that Dimorphos, like Didymos, is an S-type asteroid (Lin et al., 2023; Bagnulo et al., 2023; Gray et al., 2023; Ieva et al. 2023). While these telescopic observations provide evidence that the composition of Dimorphos is the same as that of Didymos, the density of the objects could still be different depending on the macroporosity of the bodies. Thus, the analysis considered a range for the density of Dimorphos from 1500 to 3300 kg/m^3, with a preferred estimate of the density of Dimorphos of 2400 kg/m^3, given the knowledge of the Didymos system at the time (Cheng et al., 2023a).

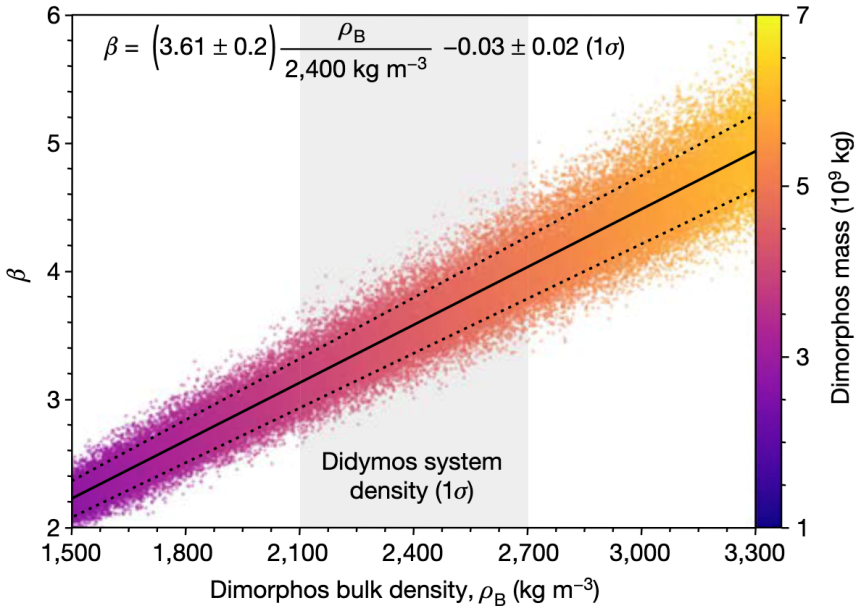

Figure 18. β as a function of Dimorphos' bulk density ρ_β from the dynamical Monte Carlo analysis. Individual samples are plotted as points, the linear fit for the mean β is plotted as a solid line, and the dotted lines show the 1σ confidence interval. The color bar indicates the mass of Dimorphos corresponding to each Monte Carlo sample, which is determined by bulk density and the volume. The density range shown corresponds to the 3σ range of the Didymos system density, and the shaded region highlights the 1σ range. If the density of Dimorphos were 2400 kg/m^3, β = 3.61, −0.25, +0.19 (1σ). From Cheng et al. (2023a).

From the Monte Carlo approach, an instantaneous reduction in Dimorphos' along-track orbital velocity component of 2.70 ± 0.10 mm/s (1σ) was calculated (Cheng et al., 2023a). Considering the full range of plausible Dimorphos densities, the calculation of β yielded a range of values from 2.4 to 4.9, as shown in Figure 18 (Cheng et al., 2023a). If Dimorphos is assumed to have a density of 2400 kg/m^3, then the resulting β value is 3.6 (Cheng et al., 2023a). The largest uncertainty in the β value resulting from DART's kinetic impact test is due to the uncertainty in the mass of Dimorphos. Thus, minor refinements in the shape of Dimorphos (Daly et al., 2023b) or the period change caused by DART's impact (Naidu et al., 2023; Scheirich et al., 2023) that have occurred since this initial calculation of β (Cheng et al., 2023a) do not have a significant impact on this overall result (Richardson et al., 2023). The determination of the β value produced from DART's kinetic impact test achieved the mission's DART-4A Level 1 requirement.

The range of β values determined from the DART mission are within the range of pre-impact predictions from simulations, which spanned β values from 1 to 6 (Stickle et al., 2022; Raducan and Jutzi 2022). Experiments have also determined a comparable range of β values, including an experiment with a target that was a collection of stones to mimic a rubble pile and resulted in a β value of 3.4 (Walker et al., 2022). While there is uncertainty in the β value because of the unknown mass of Dimorphos, the full range of β values determined for the DART experiment is >2, indicating that more momentum was transferred to Dimorphos from the escaping impact ejecta than was incident with the DART spacecraft. The β value is key to informing the strategy of a kinetic impactor approach to mitigate a future asteroid impact threat to Earth. Should a β value >2 be valid across a wide range of asteroids, it would mean important performance improvements for kinetic impactor asteroid deflection missions.

3.1.5 *DART-4B: Investigate the Didymos–Dimorphos system and the results of DART's impact*

In addition to DRACO and LICIACube images, images were obtained from the more than five dozen telescopes on all seven continents and in space that participated in the 2022–2023 observation campaign of the DART investigation team, as shown in Figure 19. Additionally, telescopic observations were conducted by groups that were not affiliated with the DART investigation team but were working to maximize the data obtained from DART's unique first demonstration of asteroid deflection.

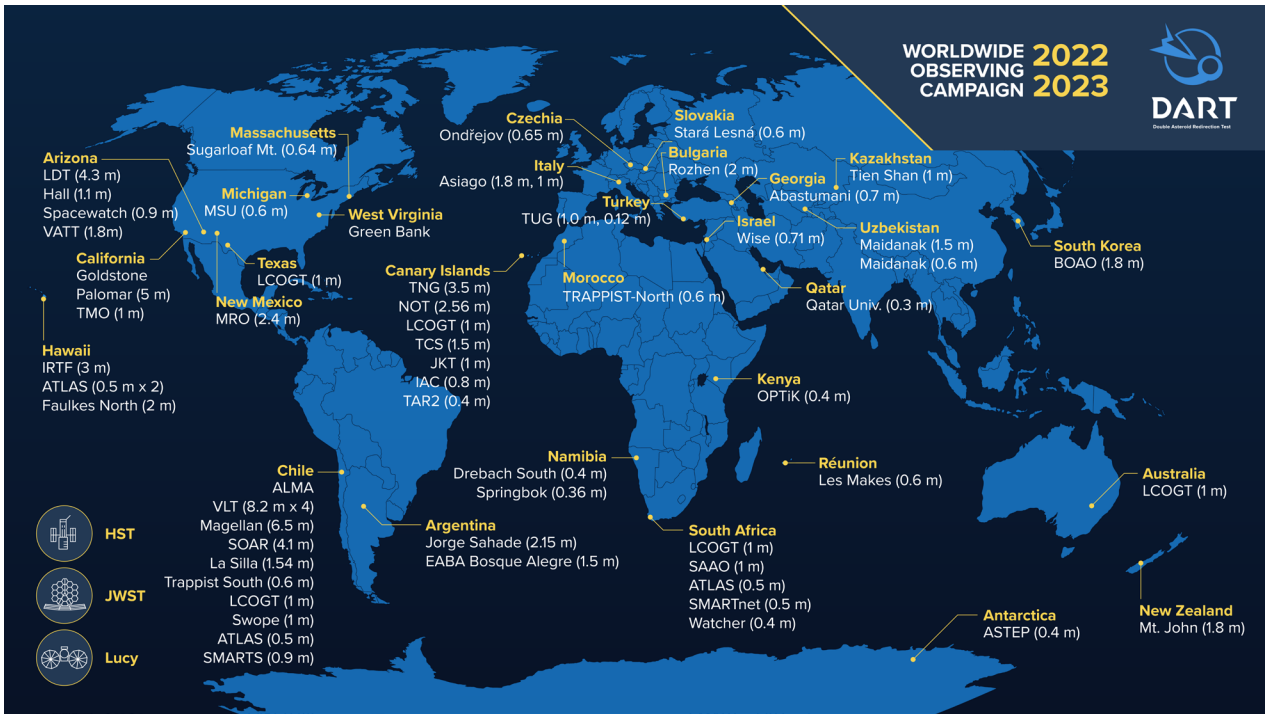

Figure 19. Map depicting the telescopic facilities on Earth and in space that contributed observations to the efforts of the DART investigation team. Numerical figures in parentheses next to telescope names indicate telescope size. Telescopes, alphabetically by location—**Antarctica:** Antarctic Search for Transiting ExoPlanets (ASTEP). **Argentina:** Jorge Sahade Telescope at the El Leoncito Astronomical Complex; Bosque Alegre Astrophysics Station (EABA). **Arizona:** Lowell Discovery Telescope (LDT); Lowell Observatory 42-inch Hall telescope; Spacewatch, University of Arizona; Vatican Advanced Technology Telescope (VATT). **Australia:** Las Cumbres Observatory Global Telescope Network (LCOGT). **Bulgaria:** Rozhen National Astronomical Observatory. **California:** Goldstone Observatory; Palomar Observatory; Table Mountain Observatory (TMO). **Canary Islands:** Telescopio Nazionale Galileo (TNG); Nordic Optical Telescope (NOT); Las Cumbres Observatory Global Telescope Network (LCOGT); Telescopio Carlos Sánchez (TCS); Jacobus Kapteyn Telescope (JKT); Instituto de Astrofísica de Canarias (IAC); Telescopio Abierto Remoto (TAR). **Chile:** Atacama Large Millimeter Array (ALMA) Radio Telescope; Very Large Telescope (VLT); Magellan Clay Telescope; Southern Astrophysical Research Telescope (SOAR); La Silla Observatory; Las Cumbres Observatory Global Telescope Network (LCOGT); Swope Telescope; Asteroid Terrestrial-impact Last Alert System (ATLAS); Small and Moderate Aperture Research Telescope System (SMARTS); TRAnsiting Planets and PlanetesImals Small Telescope (TRAPPIST)-South. **Czechia:** Ondřejov. **Georgia:** Abastumani. **Hawaii:** NASA Infrared Telescope Facility (IRTF); Asteroid Terrestrial-impact Last Alert System (ATLAS); Faulkes North. **Israel:** Wise Observatory. **Italy:** Asiago Astrophysical Observatory. **Kazakhstan:** Tien Shan Astronomical Observatory. **Kenya:** DART-OPTiK team. **Massachusetts:** Sugarloaf Mt. **Michigan:** Michigan State University (MSU). **Morocco:** TRAnsiting Planets and PlanetesImals Small Telescope (TRAPPIST)-North. **Namibia:** Drebach South Observatory; Springbok Observatory. **New Mexico:** Magdalena Ridge Observatory (MRO). **New Zealand:** University of Canterbury Ōtehīwai Mount John Observatory. **Qatar:** Qatar University. **Réunion Island:** Les Makes Observatory. **Slovakia:** Stará Lesná Observatory. **South Africa:** Las Cumbres Observatory Global Telescope Network (LCOGT); South African Astronomical Observatory (SAAO); Asteroid Terrestrial-impact Last Alert System (ATLAS); Small Aperture Robotic Telescope Network (SMARTnet); Watcher Telescope. **South Korea:** Bohyunsan Optical Astronomy Observatory (BOAO). **Space:** Hubble Space Telescope (HST); James Webb Space Telescope (JWST); NASA's Lucy mission spacecraft. **Texas:** Las Cumbres Observatory Global Telescope Network (LCOGT). **Turkey:** TÜBİTAK National Observatory (TUG). **Uzbekistan:** Maidanak Observatory. **West Virginia:** Green Bank Observatory.

Given the wide-ranging results, this section is broken into four subsections below:

- LICIACube and telescopic ejecta observations
- Impact site characterization
- Modeling DART's kinetic impact event
- Properties and dynamics of the Didymos system

All of the results were combined to achieve the mission's DART-4B Level 1 requirement.

3.1.6 *LICIACube and telescopic ejecta observations*

The ejecta produced by DART's collision was observed by LICIACube, space-based imaging systems, and ground-based telescopic facilities. These observations, ranging from a spacecraft flying by the Didymos system moments after DART's impact to telescopic facilities observing Didymos for 9 months after impact, provide a rich data set and insight into the ejecta and its evolution.

LICIACube captured images both immediately before and after DART's impact and detected that brightness increased by a factor of ~5 in the LEIA pixel values as a result of DART's impact (Dotto et al., 2023). LICIACube made its closest approach to Dimorphos 168 s after DART's impact at a distance of ~58 km; LICIACube continued to image the Didymos system until 320 s after impact (Dotto and Zinzi, 2023). In total, 426 scientific images were returned, and LICIACube continued to communicate with Earth for ~1 month following its Didymos flyby, after which time communication was lost. The LICIACube images reveal a complex and heterogeneous ejecta pattern, as shown in Figure 20. By tracking ejecta features and clumps in the rays through the LICIACube images, early-evolution ejecta speeds were found to range from a few tens of meters per second up to ~500 m/s (Dotto et al., 2023). Calculations using the LICIACube images show a wide cone of ejecta, with an opening angle of ~140° (Dotto et al., 2023). In addition to revealing clumps and diffuse features, the LICIACube images show numerous individual boulders ejected from Dimorphos. As determined by mapping >90 approximately meter-size boulders, the distribution of the boulders shows clustering in an ejection

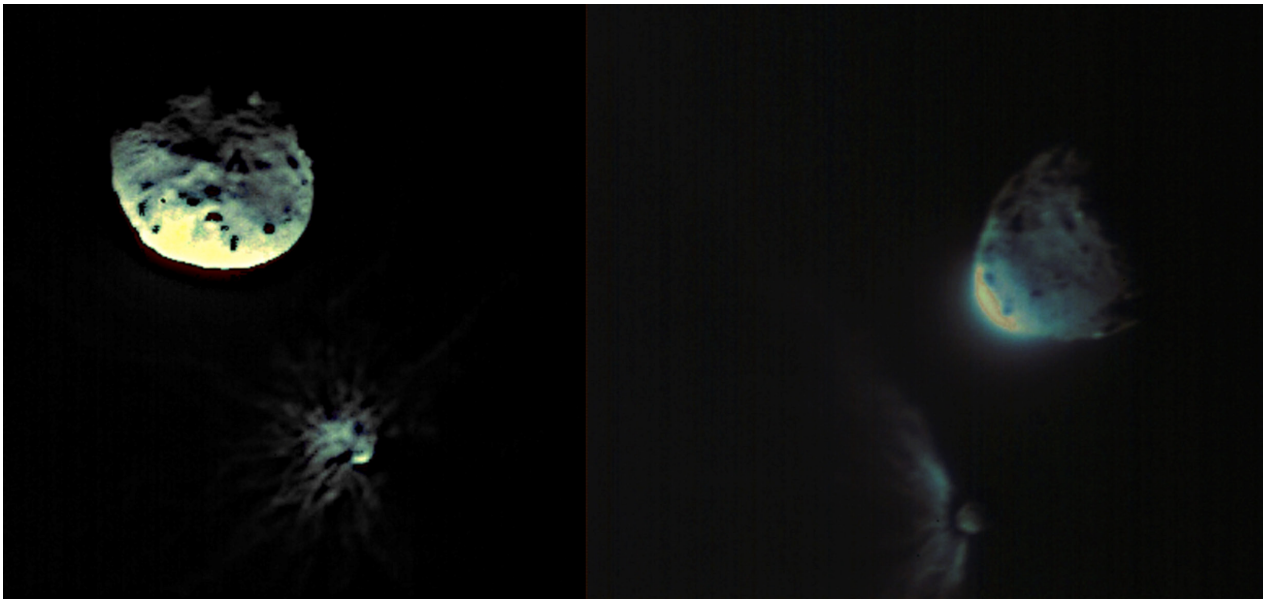

Figure 20. LICIACube imaging of DART's kinetic impact event. Left, LUKE RGB image of the targets acquired at a distance of 76 km, 8 s before closest approach (159 s after impact). Right, LUKE RGB image at a distance of 71 km, 7 s after closest approach (174 s after impact). From Dotto et al. (2023).

direction nearly perpendicular to DART's incoming trajectory, in the direction of Dimorphos' south pole, with a speed of tens of meters per second (Farnham et al., 2023).

In addition to being captured by LICIACube, the moment of DART's impact was captured by a number of Earth-based telescopes (Graykowski et al., 2023; Shestakova et al., 2023; Fitzsimmons et al., 2023), as well as the Lucy mission in space (Weaver et al., 2023) (Figure 19). An immediate fast plume of material was observed with speeds reported as ranging from ~3.6 to ~1 km/s (Weaver et al., 2023; Shestakova et al., 2023; Fitzsimmons et al., 2023; Graykowski et al., 2023). Alkali metal emissions were observed associated with DART's impact event in relative amounts close to solar system abundances—this is consistent with the fast plume being composed of material that originated from Dimorphos (Shestakova et al., 2023). The brightness of the fast plume correlated with the filter bandpass, such that Earth-based observations taken through filters that encompassed Na or K emissions observed a brighter fast plume (Fitzsimmons et al., 2023). The lower brightness Lucy observed, compared with ground-based observations, has also been attributed to the different phase-angle viewing conditions (Weaver et al., 2023). Although the fast ejecta plume contributed substantially to the overall initial brightening of the Didymos system, estimates of the mass associated with the fast ejecta plume are just a few hundreds to a few thousands of kilograms of material (Graykowski et al., 2023; Fitzsimmons et al., 2023).

In the hours after DART's impact, both the HST (Li et al., 2023) and the JWST (Thomas et al., 2023b) captured views of the Didymos system and the resulting ejecta. These telescopic observations confirmed the wide opening angle of the ejecta cone that LICIACube viewed in the minutes following impact. Analysis that combined the multiple observations and viewing conditions showed that the ejecta cone is not axially symmetric and has an elongated shape due to the curvature of Dimorphos (Hirabayashi et al., 2023). Ground-based telescopes and the HST also obtained views of the evolution of the ejecta over its first few hours, showing the change from a cone to the initial indications of a tail of material leaving the Didymos system within a few hours of DART's impact (Li et al., 2023; Opitom et al., 2023; Rozek et al., 2023; Murphy et al., 2023; Lister et al., 2023). The evolution of the ejecta is consistent with the ejecta first being dominated by the gravitational interaction between Didymos and Dimorphos as a binary system and then subsequently with the ejected dust being driven out into a tail by solar radiation pressure, as shown in Figure 21 (Li et al., 2023). Spectral and color observations (Lin et al., 2023) as well as polarimetric observations (Bagnulo et al., 2023; Gray et al., 2023) provide evidence that the ejecta excavated from Dimorphos shares similar properties to Didymos as an S-type asteroid. Observations of the ejecta tail continued for many months after DART's impact (Opitom et al., 2023; Lister et al., 2023; Kareta et al., 2023; Rozek et al., 2023; Moreno et al., 2023; Lin et al., 2023; Gray et al., 2023; Murphy et al., 2023). The ejecta tail ultimately extended over 70,000 km in length. Deep HST images acquired in December 2022 revealed a population of meter-size and larger boulders, comoving with the Didymos system with speeds consistent with being among the slowest-moving material to escape the system (Jewitt et al., 2023). The final observations of the ejecta tail were made by HST in July 2023, and they show a well-resolved ejecta tail without a clear sign of detachment. Observations of the Didymos system will be possible again in 2024, opening the possibility to continue studying the evolution of the ejecta tail created by DART's kinetic impact.

Analysis and models of the ejecta observations, informed by pre-impact studies (Fahnestock et al., 2022; Ferrari et al., 2022; Moreno et al., 2022; Rossi et al., 2022; Tancredi et al., 2022), were used to characterize the ejecta dust properties, including the particle size distribution and mass. The particle sizes in the ejecta tail are estimated to range from micrometers to a few centimeters, with radiation pressure sorting the particle size distribution along the tail (Li et al., 2023; Moreno et al., 2023; Lin et al., 2023). Observations of the reflectance slope of the evolving ejecta showed that the initial ejecta was bluer than in the pre-impact system, while the tail that formed became redder over

the weeks following impact, consistent with it being composed of larger particles (Opitom et al., 2023). Observations made with ALMA determined the thermal emission from the Didymos system and the resulting ejecta, providing an estimate for the mass of the ejecta of 1–6 × 10^7 kg (Roth et al., 2023). A total ejecta mass estimate of >10^7 kg is consistent with the mass of ejecta estimated from modeling the fading rate of Didymos over the first few weeks from optical observations (Graykowski et al., 2023) and also consistent with the results and lower limits derived from modeling the ejecta evolution (Moreno et al., 2023; Ferrari et al., 2023).

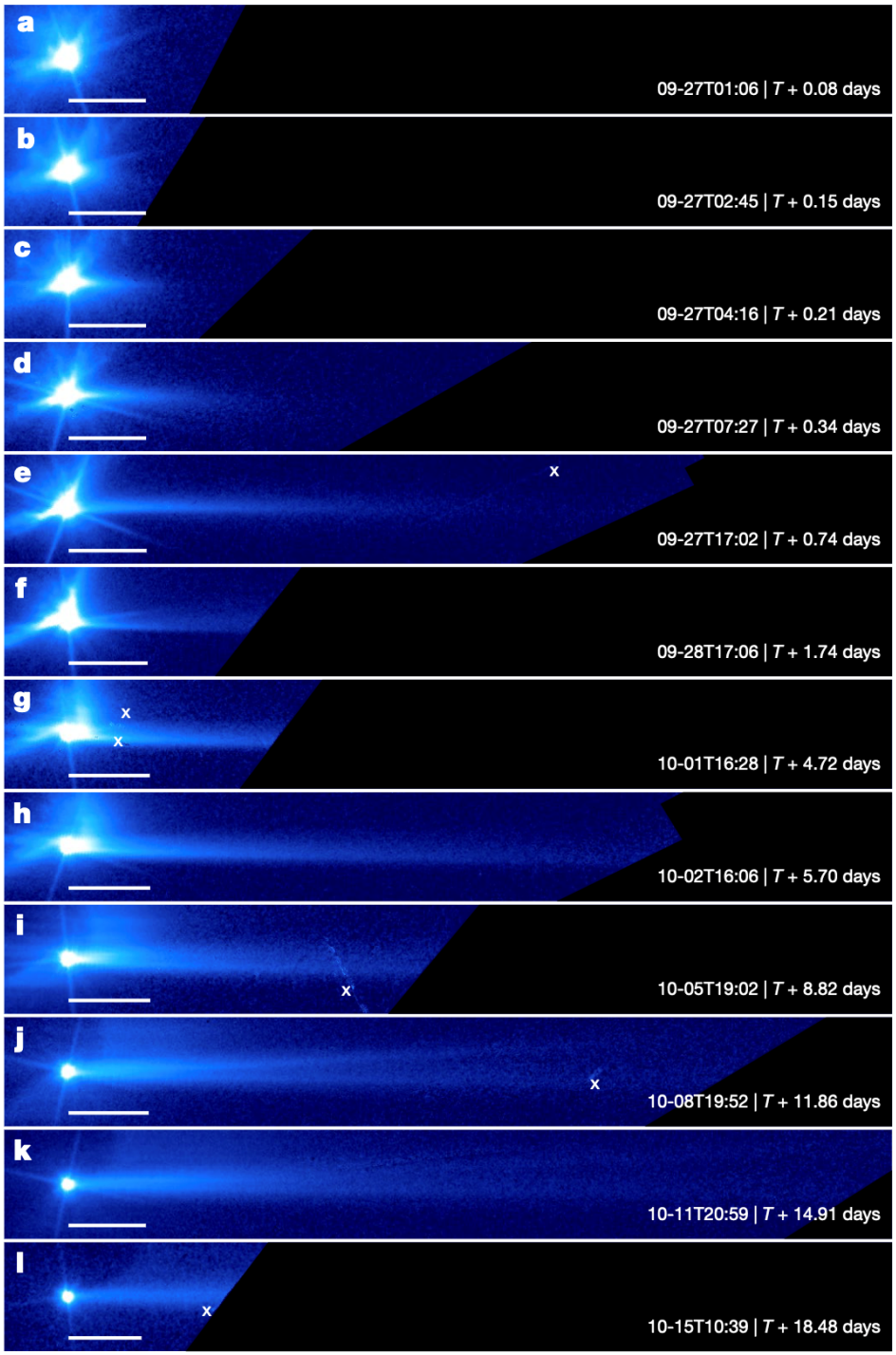

Figure 21. Tail formation from the Dimorphos ejecta cloud. a–l, All frames are rotated such that the expected direction of the tail is in the horizontal direction extending toward the right. All frames are displayed with the same logarithmic brightness scale. The x symbol marks imaging artifacts. The scale bars are aligned with the asteroid at one end and extend 200 km toward the tail direction. The first frame (a) in this sequence, acquired at *T* (time since DART impact) + 0.08 days (*T* + 1.9 h), shows no signs of a tail. A tail was visible starting from the second frame (b), acquired at *T* + 0.15 days (*T* + 3.5 h). The tail continued to grow in a direction that is, in general, consistent with an impulsive emission of dust from Dimorphos at the time of impact. i–k, A secondary tail is visible between *T* + 8.82 days and *T* + 14.91 days, pointing at about 4º north of the original tail. From Li et al., (2023).

3.1.7 *Impact site characterization*

Reconstruction of DART's trajectory into the local topography of Dimorphos shows that the DART spacecraft bus impacted between two large, ~6-m boulders, with the solar arrays impacting these boulders tens of microseconds before the main mass of the DART spacecraft (Daly, Ernst, Barnouin et al., 2023a), as shown in Figure 22. Following the International Astronomical Union (IAU)-approved nomenclature, which describes features on Didymos and Dimorphos using percussion musical instruments, in January 2023, these two boulders were named Atabaque and Bodhran. Other named features include Pūniu, a small boulder that is well resolved in the DRACO images but located farther from the impact site and is used to define the Dimorphos coordinate system; Caccavella, a 2-m boulder also near the impact site; and Dhol, the distinctive boulder seen on the limb of Dimorphos.

The shape of Dimorphos was derived from stereophotoclinometry using DRACO images, following the methods established before impact (Daly et al., 2022). The approach greatly benefited from the distinctive curvature of the terminator and from reflected light from Didymos faintly illuminating the non-sunlit surface of Dimorphos in the DRACO images (Daly et al., 2023b). Analysis of LICIACube images of Dimorphos obtained from a different viewing geometry than DRACO and illuminated by scattered light within the ejecta cloud are also consistent with this derived model of the final shape (Zinzi et al., 2023).

Calibrated DRACO images that have been projected onto the Dimorphos shape model (Daly et al., 2023b) have enabled detailed geologic investigations of Dimorphos and the DART impact site, in many cases by taking advantage of the analysis capabilities of the Small Body Mapping Tool (Ernst et al., 2018). The size–frequency distribution of boulders on Dimorphos is fit by a Weibull distribution, which suggests that the boulders might have originated from impacts but were also later modified by other processes, such as repeated impacts, thermal fragmentation, or re-accumulation processes (Pajola et al., 2023). Mapping of individual cracks seen on boulders also suggests that thermal-driven stresses are affecting the boulders on Dimorphos (Lucchetti et al., 2023). Although the surface of Dimorphos is dominated by cobbles and boulders, 12 topographic depressions have been identified as impact

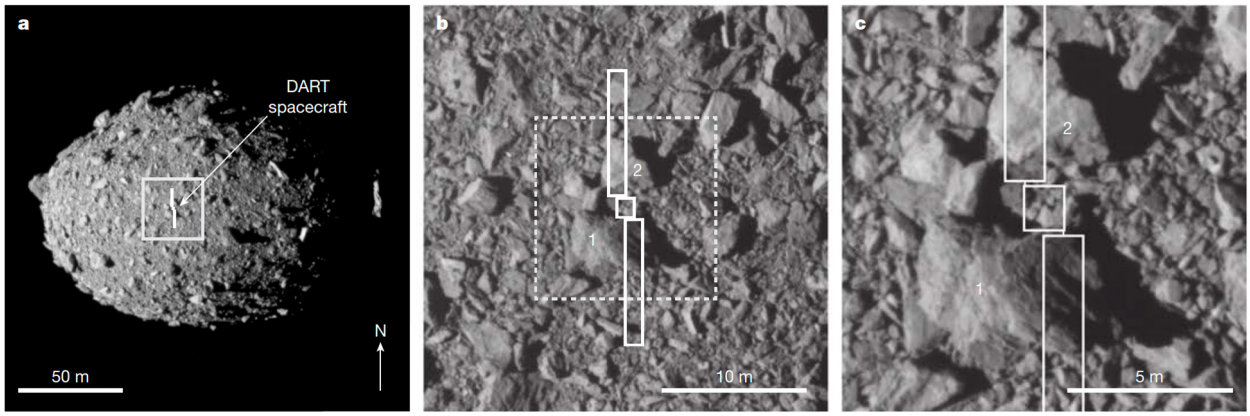

Figure 22. The asteroid Dimorphos and the DART impact site as shown in calibrated DRACO images. a, Dimorphos with an appropriately scaled and correctly oriented outline of the DART spacecraft centered on the impact site. b, A closer view of the DART impact site showing the outline of the spacecraft bus and solar arrays over the DRACO image. Note the positions of the two solar arrays relative to two large boulders, labeled 1 (6.5 m long, named Atabaque) and 2 (6.1 m long, named Bodhran). c, The spacecraft bus hit between boulders 1 and 2, whereas the solar arrays interacted with these boulders. The solid white box in a shows the location of the image in b. The dashed white box in b shows the location of the image in c. From Daly, Ernst, Barnouin et al. (2023a).

craters, ranging in size from 3 to 11 m, and a few long lineaments have been mapped on its surface (Barnouin et al., 2023). The surface geology of Dimorphos is suggestive of a loosely consolidated rubble pile, although the possibility of some larger, stronger aggregates in its interior cannot be ruled out currently, and the presence of lineaments has implications for the body's strength and subsurface structure (Barnouin et al., 2023). These geologic studies provide insight into understanding Dimorphos as it relates to DART's kinetic impact test but also into understanding the asteroid population in general, as Dimorphos is the smallest asteroid ever investigated by a spacecraft.

3.1.8 *Modeling DART's kinetic impact event*

Numerical modeling conducted after impact was informed by the shape of Dimorphos and its boulder-strewn surface and the trajectory and impact conditions of the DART spacecraft. These details were incorporated into the models' starting conditions (Raducan et al., 2023; Stickle et al., 2023; DeCoster et al., 2023). The models show that the generally complex heterogeneous nature of the ejecta rays viewed by LICIACube is consistent with DART's impact into a nonuniform surface, with the location and size of the boulders influencing the resulting ejecta pattern (Raducan et al., 2023; Stickle et al., 2023), as shown in the example in Figure 23. This is in line with laboratory observations of ray formation after impact on heterogeneous materials (Kadono et al., 2019; Ormö et al., 2022). Impact simulations have been successful at modeling the wide opening angle of the ejecta cone (Raducan et al., 2023; Stickle et al., 2023), although some models have suggested that, for cohesive strengths >500 Pa, the wide ejecta cone is poorly reproduced (Raducan et al., 2023). Impact simulations have also produced results consistent with the β values determined for DART's impact, but the models draw different conclusions for the implied strength of Dimorphos. Some models where the near-surface strength can range from near zero (~10 Pa) to "moderately weak" (tens of kilopascals) produce β values consistent with DART's results (Stickle et al., 2023), while other models conclude that cohesive strengths less than a few pascals are required to provide the best-fit outcome in terms of β and the excavation timescale (Raducan et al., 2023).

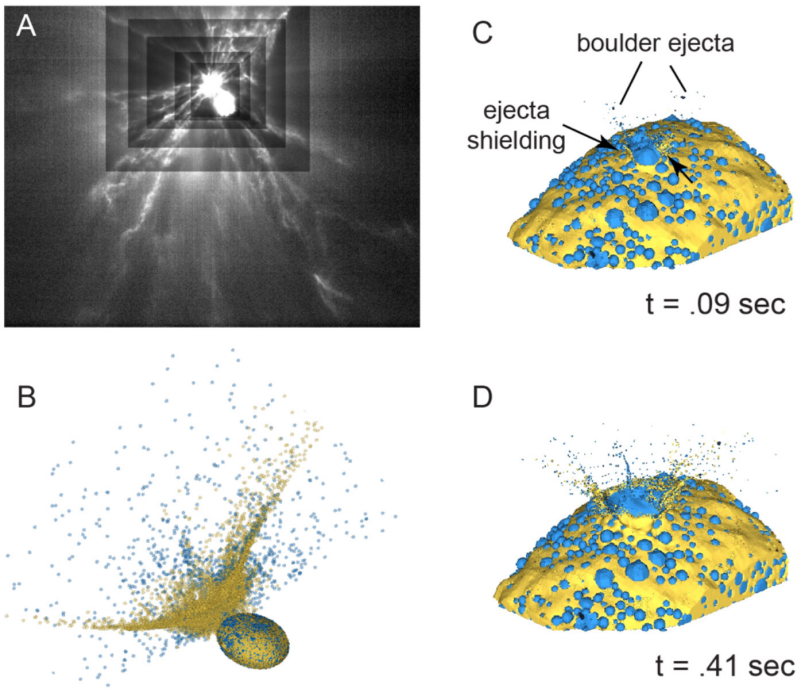

Figure 23. A, LICIACube image of ejecta after the DART impact. Each rectangle represents a different level of contrast to better show fine structure in the rays. B, Spheral simulation at 4.7 s showing a wide ejecta curtain and ejecta rays similar to those seen by LICIACube. C, CTH simulation showing development of ejecta rays very early in the cratering process (0.09 s) as a result of interaction of boulder ejecta. D, CTH simulation showing development of ejecta rays early in the cratering process (0.42 s). These rays are primarily due to heterogeneous surface morphology (boulders and/or slope). From Stickle et al. (2023).

Analysis using LICIACube images of the plume has provided constraints on Dimorphos' material properties, using the approach established in pre-impact models (Cheng et al., 2020; Cheng et al., 2022). LICIACube imaging of the ejecta plume shows no evidence for plume clearing at low altitude, and at ~3 min after DART's impact, the images show that the ejecta plume remains optically thick (Cheng et al., 2023b). Modeling efforts concluded that these LICIACube imaging results, in combination with considering the momentum enhancement that resulted from DART's impact, are consistent with models where Dimorphos' strength is <500 Pa and that the best-fit results are obtained for the 5- to 50-Pa-strength cases, which were the lowest considered in the study (Cheng et al., 2023b).

The cohesive strength also factors into predicting the outcome of DART's impact on Dimorphos' surface. For a set of simulations that suggest >10 Pa to tens of kilopascals, a crater with a diameter of ~30–60 m is predicted (Stickle et al., 2023), which is a very sizable crater on Dimorphos, whose volume-equivalent diameter is only 150 m (Daly, Ernst, Barnouin et al., 2023a). For models that suggest a strength less than a few pascals, the simulations suggest that DART's impact caused global deformation and reshaping of Dimorphos rather than a well-defined crater (Raducan et al., 2023).

The high-quality and extensive post-impact photometric observations (Moskovitz et al., 2023) provide constraints on the post-impact axial dimensions of Dimorphos, by both dynamically modeling of the orbit (Naidu et al., 2023) and directly measuring the rotational light curve of Dimorphos in a subset of the observations (Pravec et al., 2023). The estimated post-impact equatorial axis ratio of Dimorphos from modeling the orbit is 1.3 (Naidu et al., 2023), differing from the 1.02 equatorial axis ratio determined using DRACO approach images (Daly et al., 2023b). The Dimorphos rotational light curve is also suggestive of Dimorphos having axial ratios that are outside the uncertainties associated with the axial ratios determined using the pre-impact DRACO images (Daly et al., 2023b). Different post-impact axial ratios for Dimorphos could be evidence of the creation of a large crater or reshaping of the body as a result of DART's impact. Any DART-induced reshaping of Dimorphos could also perturb Dimorphos' orbit and contribute minorly to the observed period change, with implications for fully interpreting the β value due to DART's kinetic impact event (Nakano et al., 2023; Meyer et al., 2023b; Richardson et al., 2023).

3.1.9 *Properties and dynamics of the Didymos system*

Upon seeing the DRACO images, it was immediately realized that the shape of Didymos differed from that developed based on radar observations (Naidu et al., 2020). The Didymos radar shape model contained the distinctive bulge of Didymos at its equator, resulting in a "top-shape" as seen on other asteroids such as Ryugu (Watanabe et al., 2019) and Bennu (Barnouin et al., 2019). However, the X, Y, Z dimensions determined for Didymos from the radar shape model were 832 m, 838 m, and 786 m (Naidu et al., 2020). In contrast, the Didymos shape model derived by stereophotoclinometry using DRACO and LICIACube images yields X, Y, Z dimensions of 819 m, 801 m, and only 607 m (Barnouin et al., 2023). This substantial difference in the Z-axis was apparent even in the approach images of DRACO, as shown in Figure 24.

The smaller size of Didymos derived from spacecraft imaging versus radar observations affects the calculated density of Didymos, as the mass of the binary system is derived by fitting the binary orbit. DRACO imaging also provided new constraints on the separation distance of Didymos and Dimorphos before DART's impact (Thomas et al., 2023a), constraining the value to 1189 ± 17 m (Naidu et al., 2023). Both of these factors contribute to determining the density of the Didymos system. Before DART's impact, the density of the Didymos system was estimated as 2170 ± 350 kg/m^3 (Naidu et al., 2020), but using the results derived from DART mission data, the current best estimate of the Didymos system's density is considerably higher, at 2790 ± 140 kg/m^3 (Naidu et al., 2023). The mass of Didymos composes >99% of the system's mass, and hence the density of Dimorphos remains largely unconstrained by

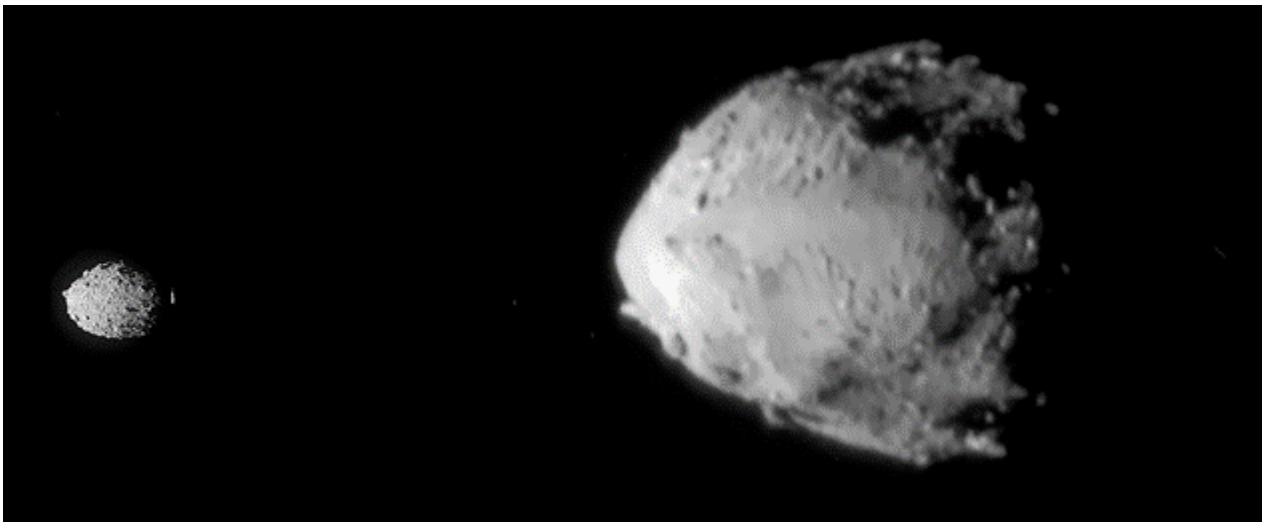

Figure 24. A mosaic of two DRACO images showing Dimorphos (left, extent in Z-axis: 115 m) and Didymos (right, extent in Z-axis: 607 m) oriented with their north poles toward the top of the image and with each asteroid and their distance to each other to scale. Credit: NASA/Johns Hopkins APL.

this calculation. However, a density of 2790 kg/m^3 for Didymos has important implications for the stability, formation, and evolution of the Didymos binary system (Richardson et al., 2023). Didymos' surface boulders and flattened shape with an equatorial ridge provide evidence that the body is a rubble pile, although its noncircular perimeter also indicates that its interior probably contains some larger distinct aggregates as well (Barnouin et al., 2023).

The geologic features on the surface of Didymos appear more varied than those of the boulder-strewn surface of Dimorphos. Three geological regions on Didymos have been mapped: one low-latitude region that possesses fewer large boulders and has a slightly lower albedo, a higher-latitude region with multiple large boulders and degraded craters, and a transition region between the two other regions (Barnouin et al., 2023). The Didymos geology correlates with its surface elevation, with the rougher terrain corresponding to highlands and the smoother terrain to lowlands (Barnouin et al., 2023). Multiple craters have been identified in the higher-latitude region, with the largest being ~270 m in diameter (Barnouin et al., 2023). Crater size–frequency analysis suggests that the surface age of Didymos is ~12.5 My and Dimorphos is <0.3 My (Barnouin et al., 2023). There is evidence for boulder tracks in the higher-latitude region, and these tracks provide constraints on the surface cohesion of Didymos (Barnouin et al., 2023). A comparison with the boulder size–frequency distributions observed on other asteroids suggests that Didymos and Dimorphos are likely the most boulder-dense asteroids visited by spacecraft to date (Pajola et al., 2023).

Pre-impact studies were important in establishing the methodologies that would be applied to investigate the post-impact dynamics of the Didymos system and in considering a wide range of possible outcomes (Agrusa et al., 2020; Agrusa et al., 2021; Agrusa et al., 2022; Makadia et al., 2022; Meyer et al., 2021; Meyer et al., 2023a; Richardson et al., 2022). Overall, the DART kinetic impact test resulted in a small change to the dynamical state of the Didymos system that is generally consistent with pre-impact expectations, with the biggest surprises attributed to the flattened shape of Didymos compared with the radar-based model and the oblate pre-impact shape of Dimorphos (Richardson et al., 2023). Modeling the dynamics of the binary system after DART's impact indicates that the semimajor axis of Dimorphos' orbit was decreased by ~37 m (Meyer et al., 2023b) and now has a value of 1152 ± 18 m (1σ) (Richardson et al. 2023). If DART's impact considerably reshaped Dimorphos,

this reshaping may place the body outside of a currently stable shape and dynamical configuration, possibly providing a reservoir of material to maintain the tail (Richardson et al., 2023). Additionally, dynamical models show that reshaping also increases the chances for Dimorphos to enter a tumbling state after DART's impact (Meyer et al., 2023b).

Models of the evolution of the ejecta suggest that ~10^6 kg of material are expected to have re-impacted Didymos or Dimorphos within the first 15 days following DART's impact (Moreno et al., 2023; Ferrari et al., 2023), with potential implications for the dynamics of the system (Richardson et al., 2023). Pre-impact studies suggested that ejecta impacting Didymos could result in reshaping of the body, which would be accompanied by a change in the rotational period of Didymos (Hirabayashi et al., 2019; Hirabayashi et al., 2022; Nakano et al., 2022); no change in the rotational period of Didymos has been detected over the months of telescopic observations that followed DART's impact event (Naidu et al., 2023; Scheirich et al., 2023), suggesting that measurable reshaping of Didymos did not occur.

No Dimorphos rotation period has been obtained from pre-impact observations. However, post-impact observations that have resolved the light curve of Dimorphos (Pravec et al., 2023) are consistent with Dimorphos being tidally locked, while also suggesting the possibility that Dimorphos entered a tumbling state (Agrusa et al., 2021; Meyer et al., 2023b), was reshaped, or both.

As it relates to the formation of the Didymos binary system, the oblate shape of Dimorphos was unexpected and is in contrast to the prolate shapes associated with other secondary members of binary asteroid systems (Richardson et al., 2023). The observation that Dimorphos does not have an irregular shape and has a boulder-covered surface is consistent with modeling its formation as quickly accreting from material shed by a fast-spinning Didymos (Madeira et al., 2023), although such a model also produces a prolate rather than oblate shape for Dimorphos. Whether Dimorphos formed with this oblate shape or evolved into this shape is an ongoing area of study to gain understanding into the formation of binary asteroid systems (Agrusa et al., 2023). The long-term dynamical evolution of a rubble-pile binary asteroid system is driven by the binary Yarkovsky–O'Keefe–Radzievskii–Paddack (YORP) effect and tides (Richardson et al., 2022). DART data have informed predictions for the effects of DART's impact event on the long-term dynamical evolution of the Didymos–Dimorphos system, although such predictions are sensitive to the exact shape of Dimorphos and the nature of any cratering or reshaping experienced (Cueva et al., 2023). A measurement of heliocentric β for the Didymos system is not yet possible, although multiple high-quality stellar occultation observations obtained in 2022–2023, including detections of Dimorphos as the smallest object ever observed during an occultation campaign, may make such a measurement possible in the next few years (Makadia et al., 2023).

4 Issues and lessons learned

As a technology demonstrator, the DART mission was heavy in technological development. While it seemed that these technologies would greatly enhance the engineering return of the mission, it became clear through the development and then operation that some of these elements (e.g., NEXT-C and ROSA) could have likewise contributed to a failure to impact Dimorphos. The quantity and operational significance of technological demonstrations should be carefully weighed against the risk to the primary objective of a mission, considering any of the "unknown unknowns" that are likely to appear with new technology. Spacecraft design should also account for these risks with more robust interfaces and minimal dependence on these systems to achieve primary mission objectives. That said, when a new technology is required for the primary mission objectives, and the development and testing is commensurate with the importance of the technology in the mission, as was the case with SMART Nav (Adams et al., 2019), the mission is greatly enhanced.

During development, the DRACO mirror-mount failure on the engineering model demonstrated a significant technical risk to maintaining an operational instrument after launch. Investigation of the issue led to process changes at APL and also to a beneficial collaboration with the NASA Goddard Space Flight Center (GSFC), whose expert assistance led to a successful redesign of the mirror support. This combination of institutional support at APL and support from outside entities (like NASA GSFC) was critical to adequately addressing this issue.

The COVID-19 pandemic also significantly impacted the project, since the project was just entering I&T at the start of the pandemic and significant build efforts were occurring across the United States on the West Coast. Aside from the parallel integration approach the team assumed to maintain the schedule for the propulsion subsystem, the colocation of key project personnel near key vendors enabled swift resolution of issues when other project personnel were unable or reluctant to travel.

Finally, during operations, the most significant concern after NEXT-C's impact on DART was the distortion between DRACO and the star tracker, which drove reduced probabilities of impact, since SMART Nav was sensitive to the alignment of the star tracker and DRACO. After an extensive test campaign, the root cause for the distortion was found to be panel heater cycling. Cycling the heaters at a higher rate to maintain temperatures improved the stability of the alignment between DRACO and the star tracker and, thus, improved predictions on the probability of impact. The star tracker noise was a top risk for DART at launch, and even required a change in a star tracker bracket angle late in the I&T flow. However, it was recognized that only in-flight data would be able to resolve of whether there was or was not an issue with the noise. Once in flight, testing confirmed that the stars were not coming in and out of the FOV of the star tracker at a rate that would introduce noise into the system, which was the worry before launch. However, other effects, such as heater cycling, became an important contribution and had to be fixed for a successful impact. Even LICIACube deployment had to be performed 5 days earlier. If the GNC team was not diligent in running down all of the various threads and threats, the mission would have had a much higher probability of a miss.

5 Conclusions

The success of the DART mission is formative for the planetary defense community, publicly highlighting not only the hazards that asteroids pose to Earth but also what humanity can do about them. The results from DART are only a single data point on what happens after a kinetic impact, specific to Dimorphos and its properties as compared with other asteroids. However, this data point is incredibly important to anchor our understanding of the behavior of celestial bodies in kinetic impact scenarios. The DART mission also showed that work with international counterparts, and the technical and scientific contributions therein, greatly enhanced the results of the mission.

The Didymos system should continue to be studied for additional dynamical changes beyond those observed during the DART mission. It is clear that the system is still evolving, and additional information may be crucial in understanding what Hera observes when it arrives at the Didymos system in the coming years. A planetary defense spacecraft to address an imminent Earth impact threat may need to be built within a much shorter time frame than DART, which poses programmatic challenges beyond those explored with DART's technology demonstration mission.

DART met all of its Level 1 requirements, and they have been documented in this final report and in peer-reviewed publications listed in the reference section and appendix. DART has also documented the fabrication and operation of its spacecraft and payload. With the investigation completed, DART has enhanced our understanding of asteroid behavior in a kinetic impact scenario and demonstrated that we have the technology to successfully deflect an asteroid by using the kinetic impactor method.

Data availability: The DART mission archive at NASA's Planetary Data System contains data from DRACO, LICIACube, and DART-supported telescopic data sets, as well as associated documentation, SPICE (Spacecraft, Planet, Instrument, Camera-matrix, Events), and advanced products, including the shape models of Didymos and Dimorphos.
(https://pds-smallbodies.astro.umd.edu/data_sb/missions/dart/index.shtml)
(https://naif.jpl.nasa.gov/pub/naif/pds/pds4/dart/dart_spice/)

The Small Body Mapping Tool (https://sbmt.jhuapl.edu/) developed by APL contains the shape models of both asteroids, with DRACO images and associated backplanes that resolve the surfaces of the asteroids.

References

Adams, E., O'Shaughnessy, D., Reinhart, M. et al. (2019). Double Asteroid Redirection Test: The Earth strikes back. *2019 IEEE Aerospace Conference*. https://doi.org/10.1109/AERO.2019.8742007

Agrusa, H.F., Richardson, D.C., Davis, A.B., et al. (2020). A benchmarking and sensitivity study of the full two-body gravitational dynamics of the DART mission target, binary asteroid 65803 Didymos. *Icarus*, *349*, 113849. https://doi.org/10.1016/j.icarus.2020.113849

Agrusa, H.F., Gkolias, I., Tsiganis, K., et al. (2021). The excited spin state of Dimorphos resulting from the DART impact. *Icarus*, *370*, 114624. https://doi.org/10.1016/j.icarus.2021.114624

Agrusa, H.F., Ferrari, F., Zhang, Y., Richardson, D.C., & Michel, P. (2022). Dynamical evolution of the Didymos-Dimorphos binary asteroid as rubble piles following the DART impact. *Planetary Science Journal*, *3*(7), 158. https://doi.org/10.3847/PSJ/ac76c1

Agrusa, H.F., Zhang, Y., Richardson, D.C., et al. (2023). Direct N-body simulations of satellite formation around small asteroids: Insights from DART's encounter with the Didymos system. *Planetary Science Journal*, submitted.

Atchison, J., Laipert, F., & McQuade, M. (2023). Double Asteroid Redirection Test (DART) final mission design and flight path control. *2023 AAS Guidance, Navigation, and Control Conference*, AAS 23-360.

Badger, A.R., John, J.W., Liang, R., et al. (2022). Dart DCIU simulator: Flight software control of the NEXT-C ion propulsion system. *International Electric Propulsion Conference*.

Bagnulo, S., Gray, Z., Granvik, M., et al. (2023). Optical spectropolarimetry of binary asteroid Didymos-Dimorphos before and after the DART impact. *Astrophysical Journal Letters*, *945*(2), L38. https://doi.org/10.3847/2041-8213/acb261

Barnouin, O.S., Daly, M.G., Palmer, E.E., et al. (2019). Shape of (101955) Bennu indicative of a rubble pile with internal stiffness. *Nature Geosciences*, *12*, 247-252. https://doi.org/10.1038/s41561-019-0330-x

Barnouin, O., Ballouz, R.-L., & Marchi, S., et al. (2023). Exploring the binary asteroid system (65803) Didymos. *Nature Communications*, submitted.

Bellerose, J., Bhaskaran, S., Rush, B., et al. (2023). Double Asteroid Redirection Test (DART): Navigating to obliteration. *Acta Astronautica*, IAA-PDC-23-146.

Cheng, A.F., Atchison, J.A., Kantsiper, B.L., et al. (2015). Asteroid Impact and Deflection Assessment mission. *Acta Astronautica*, *115*, 262-269. https://doi.org/10.1016/j.actaastro.2015.05.021

Cheng, A.F., Rivkin, A.S., Michel, P., et al. (2018). AIDA DART asteroid deflection test: Planetary defense and science objectives. *Planetary and Space Science*, *157*, 104-115. https://doi.org/10.1016/j.pss.2018.02.015

Cheng, A.F., Stickle, A.M., Fahnestock, E.G., et al. (2020). DART mission determination of momentum transfer: Model of ejecta plume observations. *Icarus*, *352*, 113989. https://doi.org/10.1016/j.icarus.2020.113989

Cheng, A.F., Raducan, S.D., Fahnestock, E.G., et al. (2022). Model of Double Asteroid Redirection Test impact ejecta plume observations. *Planetary Science Journal*, *3*(6), 131. https://doi.org/10.3847/PSJ/ac66e9

Cheng, A.F., Agrusa, H.F., Barbee, B., et al. (2023a). Momentum transfer from the DART mission kinetic impact on asteroid Dimorphos. *Nature*, *616*, 457-460. https://doi.org/10.1038/s41586-023-05878-z

Cheng, A.F., Raducan, S.D., Jutzi, M., et al. (2023b). DART impact ejecta plume evolution: Implications for Dimorphos. *Planetary Science Journal*, submitted.

Cueva, R.H., McMahon, J.W., & Meyer, A.J. (2023). The secular dynamical evolution of binary asteroid system (65803) Didymos post-DART. *Planetary Science Journal*, submitted.

Daly, R.T., Ernst, C.M., Barnouin, O.S., et al. (2022). Shape modeling of Dimorphos for the Double Asteroid Redirection Test (DART). *Planetary Science Journal*, *3*(9), 207. https://doi.org/10.3847/PSJ/ac7523

Daly, R.T., Ernst, C.M., Barnouin, O.S., et al. (2023a). Successful kinetic impact into an asteroid for planetary defence. *Nature*, *616*, 443-447. https://doi.org/10.1038/s41586-023-05810-5

Daly, R.T., Ernst, C.M., Barnouin, O.S., et al. (2023b). An updated shape model of Dimorphos from DART data. *Planetary Science Journal*, submitted.

DeCoster, M.E., Luther, R., Collins, G.S., et al. (2023). The relative effects of surface and subsurface morphology on the deflection efficiency of kinetic impactors—Implications for the DART mission. *Planetary Science Journal*, submitted.

Dotto, E., Della Corte, V., Amoroso, M., et al. (2021). LICIACube — The Light Italian CubeSat for Imaging of Asteroids in support of the NASA DART mission towards asteroid (65803) Didymos. *Planetary and Space Science*, *199*, 105185. https://doi.org/10.1016/j.pss.2021.105185

Dotto, E., Deshapriya, J.D.P., Gai, I., et al. (2023). The Dimorphos ejecta plume properties revealed by LICIACube. *Nature*, submitted.

Dotto, E., & Zinzi, A. (2023). Impact observations of asteroid Dimorphos via Light Italian CubeSat for imaging of asteroids (LICIACube). *Nature Communications*, *14*, 3055. https://doi.org/10.1038/s41467-023-38705-0

Ernst, C.M., Barnouin, O S, Daly, R.T., et al. (2018). The Small Body Mapping Tool (SBMT) for accessing, visualizing, and analyzing spacecraft data in three dimensions. *49th Lunar and Planetary Science Conference 2018 (LPSC 49)*, abstract no. 1043.

Fahnestock, E.G., Cheng, A.F., Ivanovski, S., et al. (2022). Pre-encounter predictions of DART impact ejecta behavior and observability. *Planetary Science Journal*, *3*(9), 206. https://doi.org/10.3847/PSJ/ac7fa1

Farnham, T.L., Hirabayashi, M., Deshapriya, J.D.P., et al. (2023). 3D characterization of the ejecta produced by the DART impact. *Asteroids, Comets, Meteors Conference*, no. 2127.

Ferrari, F., Raducan, S.D., Soldini, S., & Jutzi, M. (2022). Ejecta formation, early collisional processes, and dynamical evolution after the DART impact on Dimorphos. *Planetary Science Journal*, *3*(7), 177. https://doi.org/10.3847/PSJ/ac7cf0

Ferrari, F., Panicucci, P., Merisio, G., et al. (2023). Morphology of ejecta features following the DART impact on Dimorphos. *Nature Astronomy*, to be submitted.

Fitzsimmons, A., Berthier, J., Denneau, L., et al. (2023). Multi-observatory imaging of a vapor plume originating from the DART impact with Dimorphos. *Asteroids, Comets, Meteors Conference*, 2452.

Fletcher, Z.J., Ryan, K.J., Maas, B.J., et al. (2018). Design of the Didymos Reconnaissance and Asteroid Camera for OpNav (DRACO) on the Double Asteroid Redirection Test (DART). *Space Telescopes and Instrumentation 2018: Optical, Infrared, and Millimeter Wave*, *SPIE 10698*, 106981X. https://doi.org/10.1117/12.2310136

Fletcher, Z.J., Ryan, K.J., Enrst, C.M., et al. (2022). Didymos Reconnaissance and Asteroid Camera for OpNav (DRACO): Design, fabrication, test, and operation. *Space Telescopes and Instrumentation 2022: Optical, Infrared, and Millimeter Wave*, *SPIE 12180*, 121800E. https://doi.org/10.1117/12.2627873

Gray, Z., Bagnulo, S., Granvik, M., et al. (2023). Polarimetry of Didymos-Dimorphos: Unexpected long-term effects of the DART impact. *Planetary Science Journal*, submitted.

Graykowski, A., Lambert, R.A., Marchis, F., et al. (2023). Light curves and colours of the ejecta from Dimorphos after the DART impact. *Nature*, *616*, 461-464. https://doi.org/10.1038/s41586-023-05852-9

Heistand, C., Thomas, J., Tzeng, N., et al. (2019). DevOps for spacecraft flight software. *2019 IEEE Aerospace Conference*, 1-16. https://doi.org/10.1109/AERO.2019.8742143

Hirabayashi, M., Davis, A.B., Fahnestock, E.G., et al. (2019). Assessing possible mutual orbit period change by shape deformation of Didymos after a kinetic impact in the NASA-led Double Asteroid Redirection Test. *Advances in Space Research*, *63*(8), 2515-2534. https://doi.org/10.1016/j.asr.2018.12.041

Hirabayashi, M., Ferrari, F., Jutzi, M., et al. (2022). Double Asteroid Redirection Test (DART): Structural and dynamic interactions between asteroidal elements of binary asteroid (65803) Didymos. *Planetary Science Journal*, *3*(6), 140. https://doi.org/10.3847/PSJ/ac6eff

Hirabayashi, M., Farnham, T.L., Deshapriya, J.D.P., et al. (2023). Kinetic deflection change due to target shape as revealed by NASA/DART. *Science Advances*, submitted.

Ieva, S., Mazzotta Epifani, E., Dotto, E., et al. (2023). Spectroscopic characterization of the Didymos system in the aftermath of the DART event. *Nature Communications*, submitted.

Jensenius, M.A., Cheng, M., Ericksen, P., et al. (2023). SMART Nav guidance: Ensuring asteroid impact for the DART mission. *Proceedings of the 45th Annual American Astronomical Society Guidance and Control Conference*, AAS 23-135.

Jewitt, D., Kim, Y., Li, J., and Mutchler, M. (2023). The Dimorphos boulder swarm. *Astrophysical Journal Letters*, *952*, L12. https://doi.org/10.3847/2041-8213/ace1ec

John, J., Roufberg, L., Ottman, G.K., et al. (2023). NEXT-C lessons learned on the DART mission for future integration and test. *2023 IEEE Aerospace Conference*. https://doi.org/10.1109/AERO55745.2023.10116014

Kadono, T., Suetsugu, R., Arakawa, D., et al. (2019). Pattern of impact-induced ejecta from granular targets with large inclusions. *Astrophysical Journal Letters*, *880*, L30. https://doi.org/10.3847/2041-8213/ab303f

Kareta, T., Thomas, C., Li, J.-Y., et al. (2023). Ejecta evolution following a planned impact into an asteroid: The first five weeks. *Astrophysical Journal Letters*, submitted.

Li, J.-Y., Hirabayashi, M., Farnham, T.L., et al. (2023). Ejecta from the DART-produced active asteroid Dimorphos. *Nature*, *616*, 452-456. https://doi.org/10.1038/s41586-023-05811-4

Lin, Z.-Y., Vincent, J.-B., & Ip, W.-H. (2023). Physical properties of the Didymos system before and after the DART impact. *Astronomy & Astrophysics*, *676*, A116. https://doi.org/10.1051/0004-6361/202245629

Lister, T., Constantinescu, C., Gomez, E., et al. (2023). Long term monitoring of Didymos with the LCOGT network after the DART impact. *Planetary Science Journal*, to be submitted.

Lucchetti, A., Cambioni, S., Nakano, R., et al. (2023). Thermal fatigue generates boulder fractures on S-type NEA Dimorphos. *Nature Communications*, submitted.

Madeira, G., Charnoz, S., and Hyodo, R. (2023). Dynamical origin of Dimorphos from fast spinning Didymos. *Icarus*, 394, 115428. https://doi.org/10.1016/j.icarus.2023.115428

Makadia, R., Raducan, S.D., Fahnestock, E.G., & Eggl, S. (2022). Heliocentric effects of the DART mission on the (65803) Didymos binary asteroid system. *Planetary Science Journal*, *3*(8), 184. https://doi.org/10.3847/PSJ/ac7de7

Makadia, R., Chesley, S.R., Farnocchia, D., et al. (2023). Estimation of the heliocentric momentum enhancement from a kinetic impact: The Double Asteroid Redirection Test (DART) mission. *Planetary Science Journal*, submitted.

Meyer, A.J., Gkolias, I., Gaitanas, M., et al. (2021). Libration-induced orbit period variations following the DART impact. *Planetary Science Journal*, *2*(6), 242. https://doi.org/10.3847/PSJ/ac3bd1

Meyer, A.J., Scheeres, D.J., Agrusa, H.F., et al. (2023a). Energy dissipation in synchronous binary asteroids. *Icarus*, *391*, 115323. https://doi.org/10.1016/j.icarus.2022.115323

Meyer, A.J., Agrusa, H.F., Richardson, D.C., et al. (2023b). The perturbed full two-body problem: Application to post-DART Didymos. *Planetary Science Journal*, *4*, 141. https://doi.org/10.3847/PSJ/acebc7

Moskovitz, N., Thomas, C., Pravec, P., et al. (2023). Photometry of the Didymos system across the DART impact apparition. *Planetary Science Journal*, submitted.

Moreno, F., Campo Bagatin, A., Tancredi, G., Liu, P., & Domínguez, B. (2022). Ground-based observability of Dimorphos DART impact ejecta: Photometric predictions. *Monthly Notices of the Royal Astronomical Society*, *515*(2), 2178-2187. https://doi.org/10.1093/mnras/stac1849

Moreno, F., Campo Bagatin, A., Tancredi, G., et al. (2023). Characterization of the ejecta from NASA/DART impact on Dimorphos: Observations and Monte Carlo models. *Planetary Science Journal*, *4*, 138. https://doi.org/10.3847/PSJ/ace827

Murphy, B.P., Opitom, C., Snodgrass, C., et al. (2023). VLT/MUSE characterization of Dimorphos ejecta from the DART impact. *Planetary Science Journal*, submitted.

Naidu, S.P., Benner, L.A.M., Brozovic, M., et al. (2020). Radar observations and a physical model of binary near-Earth asteroid 65803 Didymos, target of the DART mission. *Icarus*, *348*, 113777. https://doi.org/10.1016/j.icarus.2020.113777

Naidu, S.P., Chesley, S.R., Farnocchia, D., et al. (2022). Anticipating the DART impact: Orbit estimation of Dimorphos using a simplified model. *Planetary Science Journal*, *3*(10), 234. https://doi.org/10.3847/PSJ/ac91c0

Naidu, S.P., Chesley, S.R., Moskovitz, N., et al. (2023). Orbital and physical characterization of Dimorphos following the DART impact. *Planetary Science Journal*, submitted.

Nakano, R., Hirabayashi, M., Agrusa, H.F., et al. (2022). NASA's Double Asteroid Redirection Test (DART): Mutual orbital period change due to reshaping in the near-Earth binary asteroid system (65803) Didymos. *Planetary Science Journal*, *3*(7), 148. https://doi.org/10.3847/PSJ/ac7566

Nakano, R., Hirabayashi, M., Raducan, S.D., et al. (2023). Dimorphos's orbit period change and attitude perturbation due to its reshaping after the DART impact. *Planetary Science Journal*, submitted.

National Academies Press (2010). *Defending Planet Earth Defending Planet Earth: Near-Earth Object Surveys and Hazard Mitigation Strategies*. https://doi.org/10.17226/12842

National Academies Press (2022). *Origins, Worlds, and Life: A Decadal Strategy for Planetary Science and Astrobiology 2023–2032*. https://doi.org/10.17226/26522

Opitom, C., Murphy, B., Snodgrass, C., et al. (2023). Morphology and spectral properties of the DART impact ejecta with VLT/MUSE. *Astronomy and Astrophysics*, *671*, L11. https://doi.org/10.1051/0004-6361/202345960

Ormö, J., Raducan, S.D., Jutzi, M., et al. (2022). Boulder exhumation and segregation by impacts on rubble-pile asteroids. *Earth and Planetary Science Letters*, *594*, 117713. https://doi.org/10.1016/j.epsl.2022.117713

Pajola, M., Tusberti, F., Lucchetti, A., et al. (2023). The boulder size-frequency distribution of a binary NEA: A Didymos origin for Dimorphos accreted blocks. *Nature Communications*, to be submitted.

Pravec, P., Thomas, C.A., Rivkin, A.S., et al. (2022). Photometric observations of the binary near-Earth asteroid (65803) Didymos in 2015-2021 prior to DART impact. *Planetary Science Journal*, *3*(7), 175. https://doi.org/10.3847/PSJ/ac7be1

Pravec, P. Scheirich, P., Meyer, A.J., et al. (2023). Dimorphos's post-impact lightcurves and constraints on its post-impact spin state and shape. *Asteroids, Comets, Meteors Conference*, no. 2052.

Raducan, S.D., & Jutzi, M. (2022). Global-scale reshaping and resurfacing of asteroids by small-scale impacts, with applications to the DART and Hera missions. *Planetary Science Journal*, *3*(6), 128. https://doi.org/10.3847/PSJ/ac67a7

Raducan, S.D., Jutzi, M., Cheng, A.F., et al. (2023). Physical properties of asteroid Dimorphos as derived from the DART impact. *Nature Astronomy*, submitted.

Richardson, D.C., Agrusa, H.F., Barbee, B., et al. (2022). Predictions for the dynamical states of the Didymos system before and after the planned DART impact. *Planetary Science Journal*, *3*(7), 157. https://doi.org/10.3847/PSJ/ac76c9

Richardson, D.C., Agrusa, H.F., Barbee, B., et al. (2023). The dynamical state of the Didymos system before and after the DART impact. *Planetary Science Journal*, submitted.

Rivkin, A.S., Chabot, N.L., Stickle, A.M., et al. (2021). The Double Asteroid Redirection Test (DART): Planetary defense investigations and requirements. *Planetary Science Journal*, *2*(5), 173. https://doi.org/10.3847/PSJ/ac063e

Rossi, A., Marzari, F., Brucato, J.R., et al. (2022). Dynamical evolution of ejecta from the DART impact on Dimorphos. *Planetary Science Journal*, *3*(5), 118. https://doi.org/10.3847/PSJ/ac686c

Roth, N.X., Milam, S.N., Remijan, A.J., et al. (2023). ALMA observations of the DART impact: Characterizing the ejecta at sub-millimeter wavelengths. *Planetary Science Journal*, in press.

Rozek, A., Snodgrass, C., Jørgensen, U.G., et al. (2023). Optical monitoring of the Didymos-Dimorphos asteroid system with the Danish telescope around the DART mission impact. *Planetary Science Journal*, submitted.

Rush, B.P., Mages, D.M., Vaughan, A.T., Bellerose, J., & Bhaskaran, S. (2023). Optical navigation for the DART mission. *33rd AAS/AIAA Space Flight Mechanics Meeting*, AAS 23-234, 1-20.

Scheirich, P., & Pravec, P. (2022). Pre-impact mutual orbit of the DART target binary asteroid (65803) Didymos derived from observations of mutual events in 2003–2021. *Planetary Science Journal*, *3*(7), 163. https://doi.org/10.3847/PSJ/ac7233

Scheirich, P. Pravec, P., Meyer, A.J., et al. (2023). Dimorphos orbit determination from mutual events photometry. *Planetary Science Journal*, submitted.

Shestakova, L.I., Serebryanskiy, A.V., Krugov, M.A., Aimanova, G.K., & Omarov, Ch. T. (2023). Signs of emissions of alkali metals Na I, Li I, and K I during first minutes after DART probe crash on Dimorphos. *Research Notes of the AAS*, 6, 223. https://doi.org/10.3847/2515-5172/ac9d33

Smith, E., Zhan, S., Adams, E., et al. (2020). Testing early and often: End-to-end testing on the Double Asteroid Redirection Test (DART). *2020 IEEE Aerospace Conference*, 1-9. https://doi.org/10.1109/AERO47225.2020.9172455

Stickle, A.M., DeCoster, M.E., Burger, C., et al. (2022). Effects of impact and target parameters on the results of a kinetic impactor: Predictions for the Double Asteroid Redirection Test (DART) mission. *Planetary Science Journal*, *3*(11), 248. https://doi.org/10.3847/PSJ/ac91cc

Stickle, A.M., Kumamoto, K.M., DeCoster, M.E., et al. (2023). Dimorphos's material properties and estimates of crater size from the DART impact. *Nature Geoscience*, submitted.

Tancredi, G., Liu, P-Y, Campo-Bagatin, A., Moreno, F., & Domínguez, B. (2022). Lofting of low-speed ejecta produced in the DART experiment and production of a dust cloud. *Monthly Notices of the Royal Astronomy Society*, *522*(2), 2403-2414. https://doi.org/10.1093/mnras/stac3258

Thomas, C.A., Naidu, S.P., Scheirich, P., et al. (2023a). Orbital period change of Dimorphos due to the DART kinetic impact. *Nature*, *616*, 448-451. https://doi.org/10.1038/s41586-023-05805-2

Thomas, C.A., Rivkin, A.S., Wong, I., et al. (2023b). JWST MIRCAM observations of the Didymos-Dimorphos system. *Asteroids, Comets Meteors Conference*, 2588.

Walker, J.D., Chocron, S., Grosch, D.J., Marchi, S., & Alexander A.M. (2022). Momentum enhancement from a 3 cm diameter aluminum sphere striking a small boulder assembly at 5.4 km s^{-1}. *Planetary Science Journal*, *3*(9), 215. https://doi.org/10.3847/PSJ/ac854f

Watanabe, S., Hirabayashi, M., Hirata, N., et al. (2019). Hayabusa2 arrives at the carbonaceous asteroid 162173 Ryugu – A spinning top-shaped rubble pile. *Science*, *364*(6437), 268-272. https://doi.org/10.1126/science.aav8032

Weaver, H.A., Spencer, J.R., Mottola, S., et al. (2023). Lucy observations of the DART impact event. *Planetary Science Journal*, to be submitted.

Zinzi, A. Hasselmann, P., Gai, I., et al. (2023). VADER: Looking for the dark side of Dimorphos with LICIACube. *Planetary Science Journal*, submitted.

Appendix 1. DART publications

2023

Agrusa, H.F., Zhang, Y., Richardson, D.C., et al. (2023). Direct N-body simulations of satellite formation around small asteroids: Insights from DART's encounter with the Didymos system. *Planetary Science Journal*, submitted.

Atchison, J., Bellerose, J., Bhaskaran, S., Laipert, F., Mages, D., McElrath, T., McQuaide, M., Mottinger, N., Rush, B., Tarzi, Z., Vaughan, A., Velez, D. (2023). DART mission design and navigation lessons learned for future planetary defense missions. *IAA Planetary Defense Conference*, Apr. 2023. IAA-PDC-23-154.

Atchison, J.A., Laipert, F.E., McQuaide, M.E., (2023). Double Asteroid Redirection Test (DART) final mission design and flight path control. *45th Rocky Mountain AAS GN&C Conference*, Feb. 2023, AAS 23-360.

Badger, A.R., John, J.W., Liang, R., et al. (2022). Dart DCIU simulator: Flight software control of the NEXT-C ion propulsion system. *International Electric Propulsion Conference*.

Bagnulo, S., Gray, Z., Granvik, M., et al. (2023). Optical spectropolarimetry of binary asteroid Didymos-Dimorphos before and after the DART impact. *Astrophysical Journal Letters*, *945*(2), L38. https://doi.org/10.3847/2041-8213/acb261

Barnouin, O., Ballouz, R.-L., Marchi, S., et al. (2023). Exploring the binary asteroid system (65803) Didymos. *Nature Communications*, submitted.

Bellerose, J., Bhaskaran, S., Rush, B., et al. (2023). Double Asteroid Redirection Test (DART): Navigating to obliteration. *Acta Astronautica*, IAA-PDC-23-146.

Bigot, J., Lombardo, P., Murdoch, N., et al. (2023). The bearing capacity of asteroid (65803) Didymos estimated from boulder tracks. *Nature Communications*, to be submitted.

Buratti, B., Pittichova, J., Mishra, I., et al. (2023). Pre-impact albedo map and photometric properties of the (65803) Didymos asteroid binary system from DART and ground-based data *Planetary Science Journal*, submitted.

Campo Bagatin, A. (2023). DART's asteroid bullseye. *Nature Geoscience*, *16*, 390–392. https://doi.org/10.1038/s41561-023-01179-2

Chabot, N.L., Rivkin, A.S., Cheng, A.F., et al. (2023). Achievement of the planetary defense investigations of the Double Asteroid Redirection Test (DART) mission. *Planetary Science Journal*, submitted.

Cheng, A.F., Agrusa, H.F., Barbee, B., et al. (2023). Momentum transfer from the DART mission kinetic impact on asteroid Dimorphos. *Nature*, *616*, 457-460. https://doi.org/10.1038/s41586-023-05878-z

Cheng, A.F., Raducan, S.D., Jutzi, M., et al. (2023). DART impact ejecta plume evolution: Implications for Dimorphos. *Planetary Science Journal*, submitted.

Cueva, R.H., McMahon, J.W., & Meyer, A J. (2023). The secular dynamical evolution of binary asteroid system (65803) Didymos post-DART. *Planetary Science Journal*, submitted.

Daly, T.R., Ernst, C.M., Barnouin, O.S., et al. (2023). Successful kinetic impact into an asteroid for planetary defence. *Nature*, *616*, 443-447. https://doi.org/10.1038/s41586-023-05810-5

Daly, T.R., Ernst, C.M., Barnouin, O.S., et al. (2023). An updated shape model of Dimorphos from DART data. *Planetary Science Journal*, submitted.

DeCoster, M.E., Luther, R., Collins, G.S., et al. (2023). The relative effects of surface and subsurface morphology on the deflection efficiency of kinetic impactors—Implications for the DART mission. *Planetary Science Journal*, submitted.

DeCoster, M.E., Stickle, A.M., Rainey, E.S.G., & Graninger, D. (2023). The effect of rubble pile morphology on momentum enhancement from a kinetic impactor. *Planetary Science Journal*, to be submitted.

Deshapriya, J.D.P., Hasselmann, P.H., Gai, I., et al. (2023). Characterization of DART impact ejecta plume on Dimorphos from LICIACube observations. *Planetary Science Journal*, submitted.

Dotto, E., Deshapriya, J.D.P., Gai, I., et al. (2023). The Dimorphos ejecta plume properties revealed by LICIACube. *Nature*, submitted.

Dotto, E., & Zinzi, A. (2023). Impact observations of asteroid Dimorphos via Light Italian CubeSat for imaging of asteroids (LICIACube). *Nature Communications*, *14*, 3055. https://doi.org/10.1038/s41467-023-38705-0

Ferrari, F., Panicucci, P., Merisio, G., et al. (2023). Morphology of ejecta features following the DART impact on Dimorphos. *Nature Astronomy*, to be submitted.

Graninger, D., Stickle, A., Owen, J.M., & Syal, M. (2023). Simulating hypervelocity impacts into rubble pile structures for planetary defense. *International Journal of Impact Engineering*, *180*, 104670. https://doi.org/10.1016/j.ijimpeng.2023.104670

Gray, Z., Bagnulo, S., Granvik, M., et al. (2023). Polarimetry of Didymos-Dimorphos: Unexpected long-term effects of the DART impact. *Planetary Science Journal*, submitted.

Hasselmann, P.H., Della Corte, V., Pravec, P., et al. (2023). The unusal brightness phase curve of (65803) Didymos. *Planetary Science Journal*, to be submitted.

Hirabayashi, M., Farnham, T.L., Deshapriya, J.D.P., et al. (2023). Kinetic deflection change due to target shape as revealed by NASA/DART. *Science Advances*, submitted.

Ieva, S., Mazzotta Epifani, E., Dotto, E., et al. (2023). Spectroscopic characterization of the Didymos system in the aftermath of the DART event. *Nature Communications*, submitted.

Ivanovski, S.L., Lucchetti, A., Zanotti, G., et al. (2023). Dust dynamics of asteroid ejecta: I. Modeling dust plume evolution after the DART impact in support of the LICIACube and DART science. *Planetary Science Journal*, submitted.

Jensenius, M.A., Cheng, M., Ericksen, P., et al. (2023). SMART Nav guidance: Ensuring asteroid impact for the DART mission. *Proceedings of the 45th Annual American Astronomical Society Guidance and Control Conference*, AAS 23-135.

John, J., Roufberg, L., Ottman, G.K., et al. (2023). NEXT-C lessons learned on the DART mission for future integration and test. *2023 IEEE Aerospace Conference*. https://doi.org/10.1109/AERO55745.2023.10116014

Kareta, T., Thomas, C., Li, J.-Y., et al. (2023). Ejecta evolution following a planned impact into an asteroid: The first five weeks. *Astrophysical Journal Letters*, submitted.

Lazzarin, M., La Forgia, F., Migliorini, A., et al. (2023). The near-Earth Didymos-Dimoprhos binary system after the NASA/DART impact: rotationally resolved spectral characterization. *Planetary Science Journal*, to be submitted.

Li, J.-Y., Hirabayashi, M., Farnham, T.L., et al. (2023). Ejecta from the DART-produced active asteroid Dimorphos. *Nature*, *616*, 452-456. https://doi.org/10.1038/s41586-023-05811-4

Lin, Z.-Y., Vincent, J.-B., & Ip, W.-H. (2023). Physical properties of the Didymos system before and after the DART impact. *Astronomy & Astrophysics*, in press. https://doi.org/10.1051/0004-6361/202245629

Lister, T., Constantinescu, C., Gomez, E., et al. (2023). Long term monitoring of Didymos with the LCOGT network after the DART impact. *Planetary Science Journal*, to be submitted.

Liu, P.-Y., Campo Bagatin, A., Benavidez, P.G., & Richardson, D.C. (2023). Deformation and partial resurfacing of Dimorphos following the DART impact. *Icarus*, submitted.

Lolachi, R., Glenar, D.A., Stubbs, T.J., & Kolokolova, L. (2023). Optical characterization of the DART impact plume: Importance of realistic ejecta scattering properties. *Planetary Science Journal*, *4*, 24. https://doi.org/10.3847/PSJ/aca968

Lucchetti, A., Cambioni, S., Nakano, R., et al. (2023). Thermal fatigue generates boulder fractures on S-type NEA Dimorphos. *Nature Communications*, submitted.

Makadia, R., Chesley, S.R., Farnocchia, D., et al. (2023). Estimation of the heliocentric momentum enhancement from a kinetic impact: The Double Asteroid Redirection Test (DART) mission. *Planetary Science Journal*, submitted.

Meyer, A.J., Agrusa, H.F., Richardson, D.C., et al. (2023). The perturbed full two-body problem: Application to post-DART Didymos. *Planetary Science Journal*, *4*, 141. https://doi.org/10.3847/PSJ/acebc7

Miller, S.E., Pittelkau, M., Superfin, E., et al. (2023). In-orbit assessment of a physics-based star tracker model using DART and PSP flight data. *Proceedings of the 12th International ESA GNC and ICATT Conference*, June 2023.

Moreno, F., Campo Bagatin, A., Tancredi, G., et al. (2023). Characterization of the ejecta from NASA/DART impact on Dimorphos: Observations and Monte Carlo models. *Planetary Science Journal*, *4*, 138. https://doi.org/10.3847/PSJ/ace827

Moskovitz, N., Thomas, C., Pravec, P., et al. (2023). Photometry of the Didymos system across the DART impact apparition. *Planetary Science Journal*, submitted.

Murphy, B.P., Opitom, C., Snodgrass, C., et al. (2023). VLT/MUSE characterization of Dimorphos ejecta from the DART impact. *Planetary Science Journal*, submitted.

Naidu, S.P., Chesley, S.R., Moskovitz, N., et al. (2023). Orbital and physical characterization of Dimorphos following the DART impact. *Planetary Science Journal*, submitted.

Nakano, R., Hirabayashi, M., Raducan, S.D., et al. (2023). Dimorphos's orbit period change and attitude perturbation due to its reshaping after the DART impact. *Planetary Science Journal*, submitted.

Opitom, C., Murphy, B., Snodgrass, C., et al. (2023). Morphology and spectral properties of the DART impact ejecta with VLT/MUSE. *Astronomy and Astrophysics*, *671*, L11. https://doi.org/10.1051/0004-6361/202345960

O'Shaughnessy, D.J. and Hefter, S. (2023). DART guidance, navigation, and control system overview, challenges, and triumphs. *2023 AAS Guidance, Navigation, and Control Conference*, Feb. 7, 2023, AAS 23-183.

Pajola, M., Tusberti, F., Lucchetti, A., et al. (2023). The boulder size-frequency distribution of a binary NEA: A Didymos origin for Dimorphos accreted blocks. *Nature Communications*, to be submitted.

Peña-Asensio, E., Küppers, M., Trigo-Rodríguez, J.M., & Rimola, A. (2023). Delivery of DART impact ejecta to Mars and Earth: Mid-term dynamical evolution. *Planetary Science Journal*, submitted.

Penttilä, A., Muinonen, K., Granvik, M., at al. (2023). Modeling linear polarization of the Didymos-Dimorphos system before and after the DART impact. *Planetary Science Journal*, submitted.

Polishook, D., DeMeo, F.E., Burt, B.J., et al. (2023). Near-IR spectral observations of the Didymos system — Daily evolution before and after the DART impact indicates Dimorphos originated from Didymos. *Planetary Science Journal*, submitted.

Raducan, S.D., Jutzi, M., Cheng, A.F., et al. (2023). Physical properties of asteroid Dimorphos as derived from the DART impact. *Nature Astronomy*, submitted.

Raducan, S.D., Jutzi, M., Mainzer, A., et al. (2023). Lessons learned from NASA's DART impact about disrupting rubble-pile asteroids. *Planetary Science Journal*, to be submitted.

Richardson, D.C., Agrusa, H.F., Barbee, B., et al. (2023). The dynamical state of the Didymos system before and after the DART impact. *Planetary Science Journal*, submitted.

Rivkin, A.S., & Cheng, A.F. (2023). Planetary defense with the Double Asteroid Redirection Test (DART) mission and prospects. *Nature Communications*, *14*, 1003. https://doi.org/10.1038/s41467-022-35561-2

Rivkin, A.S., Thomas, C.A., Wong, I., et al. (2023). Near to mid-infrared spectroscopy of (65803) Didymos as observed by JWST: Characterization observations supporting the Double Asteroid Redirection Test. *Planetary Science Journal*, submitted.

Robin, C.Q., Murdoch, N., Duchene, A., et al. (2023). Mechanical properties of rubble pile asteroids: insights from a morphological analysis of surface boulders. *Nature Communications*, submitted.

Roth, N.X., Milam, S.N., Remijan, A.J., et al. (2023). ALMA observations of the DART impact: Characterizing the ejecta at sub-millimeter wavelengths. *Planetary Science Journal*, in press.

Rożek, A., Snodgrass, C., Jørgensen, U.G., et al. (2023). Optical monitoring of the Didymos-Dimorphos asteroid system with the Danish telescope around the DART mission impact. *Planetary Science Journal*, submitted.

Rush, B.P., Mages, D.M., Vaughan, A.T., Bellerose, J., & Bhaskaran, S. (2023). Optical navigation for the DART mission. *33rd AAS/AIAA Space Flight Mechanics Meeting*, AAS 23-234, 1-20.

Scheirich, P. Pravec, P., Meyer, A.J., et al. (2023). Dimorphos orbit determination from mutual events photometry. *Planetary Science Journal*, submitted.

Shapiro, B.N. and Rodovskiy, L. (2023). DART flexible solar array and sun pointing control interactions. *45th Rocky Mountain AAS GN&C Conference*, Feb. 2023, AAS 23-181.

Stickle, A.M., Kumamoto, K.M., DeCoster, M.E., et al. (2023). Dimorphos's material properties and estimates of crater size from the DART impact. *Nature Geoscience*, submitted.

Superfin, E.A., O'Shaughnessy, D., Mages, D., et al. (2023). Line of sight error characterization and mitigations on the DART mission. *2023 AAS Guidance, Navigation, and Control Conference*, Feb. 7, 2023, AAS 23-096.

Thomas, C.A., Naidu, S.P., Scheirich, P., et al. (2023). Orbital period change of Dimorphos due to the DART kinetic impact. *Nature*, *616*, 448-451. https://doi.org/10.1038/s41586-023-05805-2

Trógolo, N., Campo Bagatin, A., Moreno, F., & Benavidez, P.G. (2023). Lifted particles from the fast spinning primary of the Near-Earth Asteroid (65803) Didymos. *Icarus*, *397*, 115521. https://doi.org/10.1016/j.icarus.2023.115521

Tropf, B.T., Haque, M., Behrooz, N., and Krupiarz, C., (2023). The DART Autonomy System. *2023 IEEE International Conference on Space Mission Challenges for Information Technology (SMC-IT)*. https://doi.org/10.1109/SMC-IT56444.2023.00020.

Vincent, J.-B., Asphaug, E., Varnouin, O., et al. (2023). Macro-scale roughness reveals the complex history of asteroids Didymos and Dimorphos. *Nature Communications*, submitted.

Walker, J.D., Chocron, S., Grosch, D.J., Marchi, S., & Alexander, A.M. (2023). Momentum enhancement from 3-cm diameter aluminum sphere impacts into iron and rock at 5 km/s. *International Journal of Impact Engineering*, *180*, 104694. https://doi.org/10.1016/j.ijimpeng.2023.104694

Waller, C.D., Espititu, R.C., Tinsman, C., et al. (2023). Science product pipelines and archive architecture for the DART mission. *Planetary Science Journal*, submitted.

Weaver, H.A., Spencer, J.R., Mottola, S., et al. (2023). Lucy observations of the DART impact event. *Planetary Science Journal*, to be submitted.

Zinzi, A. Hasselmann, P., Gai, I., et al. (2023). VADER: Looking for the dark side of Dimorphos with LICIACube. *Planetary Science Journal*, submitted.

2022

Agrusa, H.F., Ballouz, R., Meyer, A.J., et al. (2022). Rotation-induced granular motion on the secondary component of binary asteroids: Application to the DART impact on Dimorphos. *Astronomy & Astrophysics*, *664*, L3. https://doi.org/10.1051/0004-6361/202244388

Agrusa, H.F., Ferrari, F., Zhang, Y., Richardson, D.C., & Michel, P. (2022). Dynamical evolution of the Didymos-Dimorphos binary asteroid as rubble piles following the DART impact. *Planetary Science Journal*, *3*(7), 158. https://doi.org/10.3847/PSJ/ac76c1

Cheng, A.F., Raducan, S.D., Fahnestock, E.G., et al. (2022). Model of Double Asteroid Redirection Test impact ejecta plume observations. *Planetary Science Journal*, *3*(6), 131. https://doi.org/10.3847/PSJ/ac66e9

Daly, R.T., Ernst, C.M., Barnouin, O.S., et al. (2022). Shape modeling of Dimorphos for the Double Asteroid Redirection Test (DART). *Planetary Science Journal*, *3*(9), 207. https://doi.org/10.3847/PSJ/ac7523

Fahnestock, E.G., Cheng, A.F., Ivanovski, S., et al. (2022). Pre-encounter predictions of DART impact ejecta behavior and observability. *Planetary Science Journal*, *3*(9), 206. https://doi.org/10.3847/PSJ/ac7fa1

Ferrari, F., Raducan, S.D., Soldini, S., & Jutzi, M. (2022). Ejecta formation, early collisional processes, and dynamical evolution after the DART impact on Dimorphos. *Planetary Science Journal*, *3*(7), 177. https://doi.org/10.3847/PSJ/ac7cf0

Fletcher, Z.J., Ryan, K.J., Enrst, C.M., et al. (2022). Didymos Reconnaissance and Asteroid Camera for OpNav (DRACO): Design, fabrication, test, and operation. *Space Telescopes and Instrumentation 2022: Optical, Infrared, and Millimeter Wave*, *SPIE 12180*, 121800E. https://doi.org/10.1117/12.2627873

Hirabayashi, M., Ferrari, F., Jutzi, M., et al. (2022). Double Asteroid Redirection Test (DART): Structural and dynamic interactions between asteroidal elements of binary asteroid (65803) Didymos. *Planetary Science Journal*, *3*(6), 140. https://doi.org/10.3847/PSJ/ac6eff

Ieva, S., Mazzotta Epifani, E., Perna, D., et al. (2022). Spectral rotational characterization of the Didymos system prior to the DART impact. *Planetary Science Journal*, *3*(8), 183. https://doi.org/10.3847/PSJ/ac7f34

Kolokolova, L., Li, J., van Selous, M., Farnham, T., & Nagdimunov, L. (2022). 3D radiative transfer simulations of the ejecta plume anticipated from DART impact. *Planetary Science Journal*, *3*(11), 262. https://doi.org/10.3847/PSJ/ac9cde

Kumamoto, K.M., Owen, J.M., Bruck Syal, M., et al. (2022). Predicting asteroid material properties from a DART-like kinetic impact. *Planetary Science Journal*, *3*(10), 237. https://doi.org/10.3847/PSJ/ac93f2

Luther, R., Raducan, S.D., Burger, C., et al. (2022). Momentum enhancement during kinetic impacts in the low-intermediate-strength regime: Benchmarking and validation of impact shock physics codes. *Planetary Science Journal*, *3*(10), 227. https://doi.org/10.3847/PSJ/ac8b89

Makadia, R., Raducan, S.D., Fahnestock, E.G., & Eggl, S. (2022). Heliocentric effects of the DART mission on the (65803) Didymos binary asteroid system. *Planetary Science Journal*, *3*(8), 184. https://doi.org/10.3847/PSJ/ac7de7

Meyer, A.J., Scheeres, D.J., Agrusa, H.F., et al. (2022). Energy dissipation in synchronous binary asteroids. *Icarus*, *391*, 115323. https://doi.org/10.1016/j.icarus.2022.115323

Michel, P., Küppers, M., Campo Bagatin, A., et al. (2022). The ESA Hera mission: Detailed characterization of the DART impact outcome and of the binary asteroid (65803) Didymos. *Planetary Science Journal*, *3*(7), 160. https://doi.org/10.3847/PSJ/ac6f52

Moreno, F., Campo Bagatin, A., Tancredi, G., Liu, P., & Domínguez, B. (2022). Ground-based observability of Dimorphos DART impact ejecta: Photometric predictions. *Monthly Notices of the Royal Astronomical Society*, *515*(2), 2178-2187. https://doi.org/10.1093/mnras/stac1849

Naidu, S.P., Chesley, S.R., Farnocchia, D., et al. (2022). Anticipating the DART impact: Orbit estimation of Dimorphos using a simplified model. *Planetary Science Journal*, *3*(10), 234. https://doi.org/10.3847/PSJ/ac91c0

Nakano, R., Hirabayashi, M., Agrusa, H.F., et al. (2022). NASA's Double Asteroid Redirection Test (DART): Mutual orbital period change due to reshaping in the near-Earth binary asteroid system (65803) Didymos. *Planetary Science Journal*, *3*(7), 148. https://doi.org/10.3847/PSJ/ac7566

Ormö, J., Raducan, S.D., Jutzi, M., et al. (2022). Boulder exhumation and segregation by impacts on rubble-pile asteroids. *Earth and Planetary Science Letters*, *594*, 117713. https://doi.org/10.1016/j.epsl.2022.117713

Owen, J.M., DeCoster, M.E., Graninger, D.M., & Raducan, S.D. (2022). Spacecraft geometry effects on kinetic impactor missions. *Planetary Science Journal*, *3*(9), 218. https://doi.org/10.3847/PSJ/ac8932

Pajola, M., Barnouin, O.S., Lucchetti, A., et al. (2022). Anticipated geological assessment of the (65803) Didymos-Dimorphos system, target of the DART-LICIACube mission. *Planetary Science Journal*, *3*(9), 210. https://doi.org/10.3847/PSJ/ac880d

Poggiali, G., Brucato, J.R., Hasselmann, P.H., et al. (2022). Expected investigation of the (65803) Didymos-Dimorphos system using the RGB spectrophotometry data set from the LICIACube Unit Key Explorer (LUKE) wide-angle camera. *Planetary Science Journal*, *3*(7), 161. https://doi.org/10.3847/PSJ/ac76c4

Pravec, P., Thomas, C.A., Rivkin, A.S., et al. (2022). Photometric observations of the binary near-Earth asteroid (65803) Didymos in 2015-2021 prior to DART impact. *Planetary Science Journal*, *3*(7), 175. https://doi.org/10.3847/PSJ/ac7be1

Raducan, S.D., & Jutzi, M. (2022). Global-scale reshaping and resurfacing of asteroids by small-scale impacts, with applications to the DART and Hera missions. *Planetary Science Journal,* *3*(6), 128. https://doi.org/10.3847/PSJ/ac67a7

Raducan, S.D., Davison, T.M., & Collins, G.S. (2022). Ejecta distribution and momentum transfer from oblique impacts on asteroid surfaces. *Icarus*, *374*, 114793. https://doi.org/10.1016/j.icarus.2021.114793

Raducan, S.D., Jutzi, M., Zhang, Y., Ormö, J., and Michel, P. (2022). Reshaping and ejection processes on rubble-pile asteroids by impacts. *Astronomy & Astrophysics*, *665*, L10. https://doi.org/10.1051/0004-6361/202244807

Richardson, D.C., Agrusa, H.F., Barbee, B., et al. (2022). Predictions for the dynamical states of the Didymos system before and after the planned DART impact. *Planetary Science Journal*, *3*(7), 157. https://doi.org/10.3847/PSJ/ac76c9

Rossi, A., Marzari, F., Brucato, J.R., et al. (2022). Dynamical evolution of ejecta from the DART impact on Dimorphos. *Planetary Science Journal*, *3*(5), 118. https://doi.org/10.3847/PSJ/ac686c

Sánchez, P., Scheeres, D.J., & Quillen, A.C. (2022). Transmission of a seismic wave generated by impacts on granular asteroids. *Planetary Science Journal*, *3*(10), 245. https://doi.org/10.3847/PSJ/ac960c

Scheirich, P., & Pravec, P. (2022). Pre-impact mutual orbit of the DART target binary asteroid (65803) Didymos derived from observations of mutual events in 2003–2021. *Planetary Science Journal*, *3*(7), 163. https://doi.org/10.3847/PSJ/ac7233

Statler, T.S., Raducan, S.D., Barnouin, O.S., et al. (2022). After DART: Using the first full-scale test of a kinetic impactor to inform a future planetary defense mission. *Planetary Science Journal*, *3*(10), 244. https://doi.org/10.3847/PSJ/ac94c1

Stickle, A.M., DeCoster, M.E., Burger, C., et al. (2022). Effects of impact and target parameters on the results of a kinetic impactor: Predictions for the Double Asteroid Redirection Test (DART) mission. *Planetary Science Journal*, *3*(11), 248. https://doi.org/10.3847/PSJ/ac91cc

Tancredi, G., Liu, P-Y, Campo-Bagatin, A., Moreno, F., & Domínguez, B. (2022). Lofting of low-speed ejecta produced in the DART experiment and production of a dust cloud. *Monthly Notices of the Royal Astronomy Society*, *522*(2), 2403-2414. https://doi.org/10.1093/mnras/stac3258

Walker, J.D., Chocron, S., Grosch, D.J., Marchi, S., & Alexander A.M. (2022). Momentum enhancement from a 3 cm diameter aluminum sphere striking a small boulder assembly at 5.4 km s^{-1}. *Planetary Science Journal*, *3*(9), 215. https://doi.org/10.3847/PSJ/ac854f

Zinzi, A., Della Corte, V., Ivanovski, S.L., et al. (2022). The SSDC role in the LICIACube mission: Data management and the MATISSE tool. *Planetary Science Journal*, *3*(5), 126. https://doi.org/10.3847/PSJ/ac6509

2021

Agrusa, H.F., Gkolias, I., Tsiganis, K., et al. (2021). The excited spin state of Dimorphos resulting from the DART impact. *Icarus*, *370*, 114624. https://doi.org/10.1016/j.icarus.2021.114624

Bekker, D., Smith, R., & Tran, M.Q. (2021). Guiding DART to impact — The FPGA SoC design of the DRACO image processing pipeline. *2021 IEEE Space Computing Conference*, 122-133. https://doi.org/10.1109/SCC49971.2021.00020

Dotto, E., Della Corte, V., Amoroso, M., et al. (2021). LICIACube — The Light Italian CubeSat for Imaging of Asteroids in support of the NASA DART mission towards asteroid (65803) Didymos. *Planetary and Space Science*, *199*, 105185. https://doi.org/10.1016/j.pss.2021.105185

Meyer, A.J., Gkolias, I., Gaitanas, M., et al. (2021). Libration-induced orbit period variations following the DART impact. *Planetary Science Journal*, *2*(6), 242. https://doi.org/10.3847/PSJ/ac3bd1

Raducan, S.D., Jutzi, M., Davison, T.M., et al. (2021). Influence of the projectile geometry on the momentum transfer from a kinetic impactor and implications for the DART mission. *International Journal of Impact Engineering*, *162*, 104147. https://doi.org/10.1016/j.ijimpeng.2021.104147

Rivkin, A.S., Chabot, N.L., Stickle, A.M., et al. (2021). The Double Asteroid Redirection Test (DART): Planetary defense investigations and requirements. *Planetary Science Journal*, *2*(5), 173. https://doi.org/10.3847/PSJ/ac063e

Sanchez, P., Renouf, M., Azema, E., Mozul, R., & Dubois, F. (2021). A contact dynamics code implementation for the simulation of asteroid evolution and regolith in the asteroid environment. *Icarus*, *363*, 114441. https://doi.org/10.1016/j.icarus.2021.114441

Zhan, S., Bekker, D., Boye, J., et al. (2021). The design and verification of the DART single board computer FPGA. *2021 IEEE Aerospace Conference (50100)*, 1-11. https://doi.org/10.1109/AERO50100.2021.9438523

Zhang, Y., Michel, P., Richardson, D.C., et al. (2021). Creep stability of the DART/Hera mission target 65803 Didymos: II. The role of cohesion. *Icarus*, *362*, 114433. https://doi.org/10.1016/j.icarus.2021.114433

2020

Agrusa, H.F., Richardson, D.C., Davis, A.B., et al. (2020). A benchmarking and sensitivity study of the full two-body gravitational dynamics of the DART mission target, binary asteroid 65803 Didymos. *Icarus*, *349*, 113849. https://doi.org/10.1016/j.icarus.2020.113849

Cheng, A.F., Stickle, A.M., Fahnestock, E.G., et al. (2020). DART mission determination of momentum transfer: Model of ejecta plume observations. *Icarus*, *352*, 113989. https://doi.org/10.1016/j.icarus.2020.113989

Naidu, S.P., Benner, L.A.M., Brozovic, M., et al. (2020). Radar observations and a physical model of binary near-Earth asteroid 65803 Didymos, target of the DART mission. *Icarus*, *348*, 113777. https://doi.org/10.1016/j.icarus.2020.113777

Raducan, S.D, Davison, T.M., & Collins, G.S. (2020). The effects of asteroid layering on ejecta mass-velocity distribution and implications for impact momentum transfer. *Planetary and Space Science*, *180*, 104756. https://doi.org/10.1016/j.pss.2019.104756

Rainey, E.S.G., Stickle, A.M., Cheng, A.F., et al. (2020). Impact modeling for the Double Asteroid Redirection Test (DART) Mission. *International Journal of Impact Engineering*, *142*, 103528. https://doi.org/10.1016/j.ijimpeng.2020.103528

Smith, E., Zhan, S., Adams, E., et al. (2020). Testing early and often: End-to-end testing on the Double Asteroid Redirection Test (DART). *2020 IEEE Aerospace Conference*, 1-9. https://doi.org/10.1109/AERO47225.2020.9172455

Stickle, A.M., Bruck Syal, M., Cheng, A.F., et al. (2020). Benchmarking impact hydrocodes in the strength regime: Implications for modeling deflection by a kinetic impactor. *Icarus*, *338*, 113446. https://doi.org/10.1016/j.icarus.2019.113446

2019

Adams, E., O'Shaughnessy, D., Reinhart, M., et al. (2019). Double Asteroid Redirection Test: The Earth strikes back. *2019 IEEE Aerospace Conference*, 1-11. https://doi.org/10.1109/AERO.2019.8742007

Chabot, N.L., & Blair, S. (2019). A new era in planetary defense missions. *ROOM*, *3*(21), 94-99. https://room.eu.com/article/a-new-era-in-planetary-defence-missions

Heistand, C., Thomas, J., Tzeng, N. et al. (2019). DevOps for spacecraft flight software. *2019 IEEE Aerospace Conference*, 1-16. https://doi.org/10.1109/AERO.2019.8742143

Hirabayashi, M., Davis, A.B., Fahnestock, E.G., et al. (2019). Assessing possible mutual orbit period change by shape deformation of Didymos after a kinetic impact in the NASA-led Double Asteroid Redirection Test. *Advances in Space Research*, *63*(8), 2515-2534. https://doi.org/10.1016/j.asr.2018.12.041

Raducan, S.D., Davison, T.M., Luther, R., & Collins, G.S. (2019). The role of asteroid strength, porosity and internal friction in impact momentum transfer. *Icarus*, *329*, 282-295. https://doi.org/10.1016/j.icarus.2019.03.040

2018

Chen, M.H., Atchison, J.A., Carrelli, D.J., et al. (2018). Small-body Maneuvering Autonomous Real-Time Navigation (SMART Nav): Guiding a spacecraft to Didymos for NASA's Double Asteroid Redirection Test (DART). *Advances in the Astronautical Sciences AAS/AIAA Guidance, Navigation and Control*, *164*, 18-063.

Cheng, A.F., Rivkin, A.S., Michel, P., et al. (2018). AIDA DART asteroid deflection test: Planetary defense and science objectives. *Planetary and Space Science*, *157*, 104-115. https://doi.org/10.1016/j.pss.2018.02.015

Fletcher, Z.J., Ryan, K.J., Maas, B.J., et al. (2018). Design of the Didymos Reconnaissance and Asteroid Camera for OpNav (DRACO) on the Double Asteroid Redirection Test (DART). *Space Telescopes and Instrumentation 2018: Optical, Infrared, and Millimeter Wave*, *SPIE 10698*, 106981X. https://doi.org/10.1117/12.2310136

Michel, P., Kueppers, M., Sierks, H., et al. (2018). European component of the AIDA mission to a binary asteroid: Characterization and interpretation of the impact of the DART mission. *Advances in Space Research*, *62*, 2261-2272. https://doi.org/10.1016/j.asr.2017.12.020

Yu, Y., & Michel, P. (2018). Ejecta cloud from the AIDA space project kinetic impact on the secondary of a binary asteroid: II. Fates and evolutionary dependencies. *Icarus*, *312*, 128-144. https://doi.org/10.1016/j.icarus.2018.04.017

2017

Hirabayashi, M., Schwartz, S.R., Yu, Y., et al. (2017). Constraints on the perturbed mutual motion in Didymos due to impact-induced deformation of its primary after the DART impact. *Monthly Notices of the Royal Astronomical Society*, *472*(2), 1641-1648. https://doi.org/10.1093/mnras/stx1992

Stickle, A.M., Rainey, E.S.G., Bruck Syal, M., et al. (2017). Modeling impact outcomes for the Double Asteroid Redirection Test (DART) mission. *Procedia Engineering*, *204*, 116-123. https://doi.org/10.1016/j.proeng.2017.09.763

Yu, Y., Michel, P., Schwartz, S.R., Naidu, S.P., & Benner, L.A.M. (2017). Ejecta cloud from the AIDA space project kinetic impact on the secondary of a binary asteroid: I. Mechanical environment and dynamical model. *Icarus*, *282*, 313-325. https://doi.org/10.1016/j.icarus.2016.09.008

Zhang, Y., Richardson, D.C., Barnouin, O.S., et al. (2017). Creep stability of the proposed AIDA mission target 65803 Didymos: I. Discrete cohesionless granular physics model. *Icarus*, *294*, 98-123. http://dx.doi.org/10.1016/j.icarus.2017.04.027

2016

Atchison, J.A., Ozimek, M.T., Kantsiper, B.L., & Cheng, A.F. (2016). Trajectory options for the DART mission. *Acta Astronautica*, *123*, 330-339. http://dx.doi.org/10.1016/j.actaastro.2016.03.032

Bruck Syal, M., Owen, J.M., & Miller, P.L. (2016). Deflection by kinetic impact: Sensitivity to asteroid properties. *Icarus*, *269*, 50-61. http://dx.doi.org/10.1016/j.icarus.2016.01.010

Cheng, A.F., Michel, P., Jutzi, M., et al. (2016). Asteroid Impact & Deflection Assessment mission: Kinetic impactor. *Planetary and Space Science*, *121*, 27-35. http://dx.doi.org/10.1016/j.pss.2015.12.004

Michel, P., Cheng, A., Küppers, M., et al. (2016). Science case for the Asteroid Impact Mission (AIM): A component of the Asteroid Impact & Deflection Assessment (AIDA) mission. *Advances in Space Research*, *57*(12), 2529-2547. http://dx.doi.org/10.1016/j.asr.2016.03.031

2015

Cheng, A.F., Atchison, J.A., Kantsiper, B.L., et al. (2015). Asteroid Impact and Deflection Assessment mission. *Acta Astronautica*, *115*, 262-269. https://doi.org/10.1016/j.actaastro.2015.05.021

Stickle, A.M., Atchison, J.A., Barnouin, O.S., et al. (2015). Modeling momentum transfer from kinetic impacts: Implications for redirecting asteroids. *Procedia Engineering*, *103*, 577-584. https://doi.org/10.1016/j.proeng.2015.04.075

APL_COMM-23-04772